

## **16 Years of Ulysses Interstellar Dust Measurements in the Solar System: I. Mass Distribution and Gas-to-Dust Mass Ratio**

Harald Krüger and Peter Strub

*Max-Planck-Institut für Sonnensystemforschung, Justus-von-Liebig-Weg 3, 37077  
Göttingen, Germany*

krueger@mps.mpg.de

Eberhard Grün<sup>1</sup>

*Max-Planck-Institut für Kernphysik, Saupfercheckweg 1, 69117 Heidelberg, Germany*

and

Veerle J. Sterken<sup>2</sup>

*International Space Science Institute, Hallerstrasse 6, 3012 Bern, Switzerland*

### **ABSTRACT**

In the early 1990s, contemporary interstellar dust penetrating deep into the heliosphere was identified with the in-situ dust detector on board the Ulysses spacecraft. Between 1992 and the end of 2007 Ulysses monitored the interstellar dust stream. The interstellar grains act as tracers of the physical conditions in the local interstellar medium surrounding our solar system.

Earlier analyses of the Ulysses interstellar dust data measured between 1992 and 1998 implied the existence of a population of 'big' interstellar grains (up to  $10^{-13}$  kg; Landgraf et al. 2000; Frisch et al. 1999). The derived gas-to-dust-mass ratio was smaller than the one derived from astronomical observations, implying a concentration of interstellar dust in the very local interstellar medium (Grün and Landgraf 2000).

---

<sup>1</sup>Laboratory for Atmospheric and Space Physics, University of Colorado, Boulder, CO, 80303-7814, USA

<sup>2</sup>Max-Planck-Institut für Kernphysik, Saupfercheckweg 1, 69117 Heidelberg, Germany

In this paper we analyse the entire data set from 16 years of Ulysses interstellar dust measurements in interplanetary space. This paper concentrates on the overall mass distribution of interstellar dust. An accompanying paper (Strub et al. 2015) investigates time-variable phenomena in the Ulysses interstellar dust data, and in a third paper we present the results from dynamical modelling of the interstellar dust flow applied to Ulysses (Sterken et al. 2015). We use the latest values for the interstellar hydrogen and helium densities, the interstellar helium flow speed of  $v_{\text{ISM}\infty} = 23.2 \text{ km s}^{-1}$ , and the ratio of radiation pressure to gravity,  $\beta$ , calculated for astronomical silicates. We find a gas-to-dust-mass ratio in the local interstellar cloud of  $R_{g/d} = 193_{-57}^{+85}$ , and a dust density of  $(2.1 \pm 0.6) \times 10^{-24} \text{ kg m}^{-3}$ . For a higher inflow speed of  $26 \text{ km s}^{-1}$ , the gas-to-dust-mass ratio is 20% higher, and, accordingly, the dust density is lower by the same amount. The gas-to-dust mass ratio derived from our new analysis is compatible with the value most recently determined from astronomical observations (Slavin and Frisch 2008). We confirm earlier results that the very local interstellar medium contains 'big' (i.e.  $\approx 1 \mu\text{m}$ -sized) interstellar grains. We find a dust density in the local interstellar medium that is a factor of three lower than values implied by earlier analyses.

*Subject headings:* interstellar dust, interstellar medium, dust size distribution, heavy elements

## 1. Introduction

The term "dust" is often considered as a synonym for dirt, which is annoying and difficult to quantify. Astronomers who observe distant objects in our Galaxy and beyond have to struggle with foreground obscuration due to the zodiacal light in our Solar System, and with extinction by interstellar and even intergalactic dust. Therefore, dust is often considered a nuisance.

On the other hand, cosmic dust particles are involved in many astrophysical processes and play a crucial role in the cosmic lifecycle of matter. They trace physical and chemical processes everywhere in the Universe, ranging from the solar system at our doorstep as far out as high-redshift galaxies. Cosmic dust provides the surface for complex chemical reactions and determines the thermal, ionization and dynamical state of matter through its interaction with electromagnetic radiation, cosmic rays and gas particles. Dust is not easily controlled, it rather follows its own dynamics and disperses rapidly from its source. This aspect, however, has a positive side: Like photons, dust particles carry information

about remote processes through space and time, and the objects they originated from. This concept is called "Dust Astronomy", and modern dust observations are performed with a dust telescope on a dust observatory in space (Grün et al. 2004).

Interstellar dust became a topic of astrophysical research in the early 1930s when the existence of extinction, weakening, and scattering of starlight in the interstellar medium (ISM) was realised. At that time, astronomical observations provided the only information about the properties of dust in the ISM.

With the advent of dust detectors onboard spacecraft, it became possible to investigate dust particles in-situ. 40 years ago, analysis of the data obtained with the dust instruments flown on a couple of spacecraft suggested that contemporary interstellar dust grains can cross the heliospheric boundary and penetrate deeply into the heliosphere (Bertaux and Blamont 1976; Wolf et al. 1976).

In the 1990s, this was undoubtedly demonstrated: the dust detector onboard the Ulysses spacecraft, which measured mass, speed and approach direction of the impacting grains, identified interstellar dust grains with radius above  $0.1 \mu\text{m}$  that were flowing through the heliosphere (Grün et al. 1993, 1994, 1995b). These grains originated from the local interstellar cloud (LIC) which is the interstellar cloud surrounding our solar system. We follow the notation by Frisch et al. (1999). Details of the local interstellar setting of our solar system were also given by Redfield and Linsky (2008). The Ulysses measurements offered the opportunity to probe dust from the local interstellar cloud.

The Ulysses interstellar dust measurements were later confirmed by the Galileo (Baguhl et al. 1996; Altobelli et al. 2005) and Cassini spacecraft (Altobelli et al. 2003, 2007, 2015), and interstellar impactors were also identified in the Helios dust data (Altobelli et al. 2006). In 2006, the Stardust mission successfully brought a sample of collected interstellar grains to Earth (Westphal et al. 2014). Finally, there are recent claims of detections of interstellar grains with radio and plasma wave instruments (Belheouane et al. 2012).

Measurements of interstellar dust inside the planetary system now provide a new window for the study of diffuse interstellar matter at our doorstep. However, the interstellar dust stream in the heliosphere is strongly modified from the undisturbed flow outside the heliosphere, in particular by solar radiation effects and the Lorentz force. These modifications have to be taken into account for a proper interpolation of the interstellar dust properties to the interstellar medium outside the heliosphere where these grains originate from.

In addition to interstellar dust, various populations of dust originating from sources inside the solar system were investigated in interplanetary space with the Ulysses and Galileo dust experiments: the interplanetary dust complex which is constantly replenished by dust

from asteroids and comets (Grün et al. 1997), including  $\beta$ -meteoroids (i.e. dust particles which leave the solar system on unbound orbits due to acceleration by radiation pressure; Hamilton et al. 1996; Wehry et al. 2004), and dust stream particles expelled from the Jovian system by electromagnetic forces (Grün et al. 1998), to name only the most significant dust types studied so far. For a summary of the Ulysses dust investigations in interplanetary space see Krüger et al. (2010, references therein). See also Krüger and Grün (2009); Mann (2010); Frisch et al. (2011); Frisch and Slavin (2013) for recent reviews of measurements and modelling of interstellar dust in the heliosphere and beyond.

### 1.1. Interstellar Dust Entering the Heliosphere

The Ulysses in-situ dust measurements obtained in the 1990s showed that the motion of interstellar grains through the solar system is – within the dust measurement accuracy – parallel to the flow of neutral interstellar hydrogen and helium gas. A speed of  $26 \text{ km s}^{-1}$  was adopted in these earlier analyses (Grün et al. 1994; Baguhl et al. 1995a; Witte et al. 1996; Witte 2004). The grains which originated from the very local interstellar environment of our solar system were identified by their impact direction and impact speed, the latter being compatible with particles moving on hyperbolic heliocentric trajectories (Grün et al. 1994). Their dynamics depend on the grain size and is strongly affected by the interaction with the interplanetary magnetic field and by solar radiation pressure (Landgraf et al. 1999; Landgraf 2000; Mann and Kimura 2000; Czechowski and Mann 2003b,a; Landgraf et al. 2003; Sterken et al. 2012, 2013a, 2015). Strong filtration of small grains due to electromagnetic forces also occurs at the heliospheric boundary (Linde and Gombosi 2000), leading to a strong modification of the size distribution and fluxes of grains measured inside the heliosphere. The interstellar dust flux modulation due to grain interaction with the interplanetary magnetic field during solar minimum could be well explained by numerical simulations (Landgraf 1998, 2000; Landgraf et al. 2003).

The interstellar dust flow persists at high ecliptic latitudes above and below the ecliptic plane and even over the poles of the Sun, whereas interplanetary dust is strongly depleted at high latitudes (Grün et al. 1997). The interstellar dust flux measured at a distance of about 3 AU from the Sun is time-dependent, and the mean mass of the grains is about  $3 \times 10^{-16} \text{ kg}$  (Landgraf et al. 2000), corresponding to a grain radius of approximately  $0.3 \mu\text{m}$  (assuming a grain density of  $2.5 \text{ kg m}^{-3}$ ). The earlier analyses of the Ulysses dust measurements yielded an upstream direction of the dust flow at  $259^\circ$  ecliptic longitude and  $8^\circ$  latitude (Landgraf 1998).

Spectroscopic observations of sightlines to stars enable information of intervening dust

characteristics to be obtained. Studies of the dust impacts detected with both Ulysses and its twin dust detector on board Galileo indicated that the intrinsic size distribution of interstellar grains in the local interstellar cloud extends to grain sizes larger than those detectable by such astronomical observations (Frisch et al. 1999; Frisch and Slavin 2003; Landgraf et al. 2000; Grün and Landgraf 2000). Observations of radar meteors entering the Earth’s atmosphere at high speeds indicate the existence of even larger interstellar grains (Taylor et al. 1996; Baggaley and Neslušan 2002; Baggaley et al. 2007), although this conclusion remains under debate.

The Ulysses and Galileo interstellar dust measurements implied that the gas-to-dust mass ratio in the local interstellar cloud is higher than the standard interstellar value derived from cosmic abundances (Landgraf 1998; Frisch et al. 1999; Kimura et al. 2003b). This implied the existence of inhomogeneities in the diffuse interstellar medium on relatively small length scales ( $\ll 1$  kpc; Grün and Landgraf 2000).

Due to its unique highly inclined heliocentric trajectory and very long mission duration, Ulysses was able to monitor the interstellar dust flow through the solar system over 16 years. This time period covers more than two and a half revolutions of the spacecraft about the Sun through more than 2/3 of a complete 22-year (magnetic) solar cycle (Figure 1). Thus, Ulysses measured interstellar dust during solar minimum and solar maximum conditions of the interplanetary magnetic field (IMF).

Earlier comprehensive investigations of the interstellar impactors were mostly performed in the late 1990s and relied upon the significantly smaller data set available at the time. Until the end of the Ulysses mission, the interstellar dust data set has grown by more than a factor of two so that a complete re-analysis is worthwhile and can give new insights into, e.g., the grain dynamics inside the heliosphere and into the conditions in the local interstellar environment where these grains originate.

Recent measurements with the Interstellar Boundary Explorer (IBEX) spacecraft led to a revision of the interstellar gas flow vector (speed and direction) derived earlier from Ulysses measurements (Witte 2004, inflow speed  $v_{\text{ISM}\infty} = 26 \text{ km s}^{-1}$ ). The IBEX measurements of the interstellar flow are also more consistent with newer and independent astronomical measurements (Redfield and Linsky 2008). IBEX showed that the Sun is still located within the local interstellar cloud. The inflow speed of the interstellar medium as derived by IBEX is  $v_{\text{ISM}\infty} = 23.2 \text{ km s}^{-1}$  and the downstream flow direction is  $l_{\text{ISM}\infty} = 79^\circ$  ecliptic longitude and  $b_{\text{ISM}\infty} = -5^\circ$  ecliptic latitude (McComas et al. 2012). Given that the impact speed of the dust grains affects the mass calibration of our interstellar dust measurements, we analyse the Ulysses data in view of this reduced inflow speed. However, this speed was, like the direction, under debate (Lallement and Bertaux 2014; Wood et al. 2015; McComas et al.

2015). The higher inflow speed of  $v_{\text{ISM}\infty} = 26 \text{ km s}^{-1}$  increases our derived gas-to-dust mass ratio by about 20% (*cf.* Section 5).

This is the first in a series of three papers dedicated to the analysis of the full Ulysses data set of 16 years of interstellar dust measurements in the heliosphere. In this paper we review the mass distribution of interstellar grains detected in the heliosphere. Temporal variations in dust flux, impact direction and grain size during this time period are investigated by Strub et al. (2011, 2015), and results from modelling of grain dynamics in the context of the observations are presented by Sterken et al. (2015). In Section 2 we briefly describe the Ulysses mission, the Ulysses dust detector and its operation. In Section 3 we derive the Ulysses interstellar dust data set, and in Section 4 we obtain the mass distribution of interstellar grains and the gas-to-dust mass ratio in the local interstellar cloud. Section 5 is a discussion and in Section 6 we summarise our conclusions.

## 2. The Ulysses Dust Instrument

The Ulysses dust instrument detects individual dust particles impacting onto the sensor target, measures their mass and impact speed, and determines the impact direction (Grün et al. 1992b). Up to now Ulysses was the only space probe that left the ecliptic plane and passed over the poles of the Sun. Ulysses was launched in October 1990. After a swing-by manoeuvre at Jupiter in February 1992, the spacecraft’s orbital plane was almost perpendicular to the ecliptic plane ( $79^\circ$  inclination) with an aphelion at Jupiter and a six-year period (Figure 1). Subsequent aphelion passages occurred in April 1998 and in June 2004. This special orbit orientation allowed the dust detector on board Ulysses to unambiguously detect interstellar dust grains entering the heliosphere because the spacecraft’s orbital plane was almost perpendicular to the flow direction of the interstellar dust (Figure 1). Ulysses was operated until 2009.

A practically identical twin instrument was operated on board the Galileo spacecraft, which was launched in 1989, and between 1995 and 2003 it was the first Jupiter-orbiting spacecraft (Grün et al. 1992a). A third identical instrument (GORID), an engineering model of the Ulysses sensor, was operational in geostationary orbit on the Express telecommunication satellite between 1997 and 2002 (Drolshagen et al. 1999). Finally, the Cassini spacecraft, launched in 1997, carries the Cosmic Dust Analyzer (CDA) which is an upgrade of the Ulysses instrument that is equipped with a time-of-flight mass spectrometer (Srama et al. 2004). Cassini has been successfully measuring dust in the Saturnian system since 2004. Altogether, these four instruments very successfully collected cosmic dust measurements during more than 50 years in space.

## 2.1. Impact Ionisation

The physical mechanism most generally utilised in modern spaceborne in-situ detectors of cosmic dust is based on the measurement of the electric charge generated upon impact of a fast projectile onto a solid target (impact ionisation, Raizer 1960; Friichtenicht and Slattery 1963). It yields the highest sensitivity for the detection of dust particles in space (see Auer 2001, for a review). The electrical charge generated upon particle impact can be quantitatively calibrated to provide impact speed and mass of the grains. The impacts can be detected by several independent measurements on different instrument channels (multi-coincidence detection) which allows for a reliable dust impact detection and identification of noise events. In combination with a time-of-flight mass spectrometer an impact ionisation detector can measure the chemical composition of the impacting grains.

When a dust particle strikes a solid target with high speed ( $\gg 1 \text{ km s}^{-1}$ ), it produces a crater in the target and ejecta composed of both particle and target material. The ejecta consist of positive and negative ions, electrons, and neutral atoms and molecules originating from both projectile and target. Because of its high internal pressure, (up to 5 TPa) the ejecta cloud expands rapidly into the surrounding vacuum. As the ejecta strike sensor side walls and other surfaces, they produce secondary ions, electrons and debris which, in turn, can strike more surfaces and produce additional ejecta.

The experimental arrangement typically consists of a metal target plate and a collector (e.g. a metal grid) for either the ions or electrons of the impact plasma. The target is preferentially made of a material with a high electron yield like molybdenum, tantalum, tungsten or gold. Different electric potentials applied to the target plate and the collector generate an electric field, separating the positively and negatively charged particles of the plasma. Charge-sensitive amplifiers coupled to both the target plate and the collector register independently, but simultaneously, an impacting dust particle. The total amount of charge,  $Q$ , collected on each channel is a function of mass  $m$  and impact speed  $v$  of the particle as well as the particle's composition.  $Q$  can be described by the empirical law

$$Q \propto m^\alpha v^\gamma, \tag{1}$$

with  $\alpha \simeq 1$  and  $1.5 \lesssim \gamma \lesssim 5.5$  in the speed range  $2 \text{ km s}^{-1} \lesssim v \lesssim 70 \text{ km s}^{-1}$  (Auer 2001). In particular, for constant impact speed, the charge generated upon impact is proportional to the particle mass (Göller and Grün 1985).

The rather wide range in  $\gamma$  is due to different impact speeds, target and projectile materials and collector geometries used for the measurements. In particular, the physical processes involved are speed dependent and the impact ionisation process is often divided into three speed regimes, characterised by different values of  $\gamma$  (Stübig 2002). At speeds below

about  $6 \text{ km s}^{-1}$  surface ionisation dominates ( $3.5 \lesssim \gamma \lesssim 4.5$ ): The surfaces of the solid bodies involved in the impact process are heated by the impact shock, leading to thermal ionisation of the surfaces. In addition, ionisation of alkali contaminants on the target, having low ionisation potentials, takes place. In the high impact speed regime, above  $18 \text{ km s}^{-1}$ , target and projectile ionisation (volume ionisation) dominate ( $3.0 \lesssim \gamma \lesssim 5.5$ ). For intermediate speeds the charge yield is reduced due to energy consumption by melting and vaporisation processes ( $1.5 \lesssim \gamma \lesssim 2.5$ ).

A similar behaviour was also reported by Göller and Grün (1989). Due to the large uncertainties in the exponent and material dependencies, these authors used a value of  $\gamma = 3.5$  throughout the entire speed range to calibrate the Ulysses dust instrument. Here we use the empirical calibration curve of Grün et al. (1995b, their Table 4c) that was derived from impact experiments at a dust accelerator with iron, zinc coated silica and carbon particles.

The second important variable for the determination of the impact parameters is the rise time of the charge signal. It depends only on the impact speed of the particles (Dietzel et al. 1973). The rise time can be used to determine the impact speed when it is in the range of  $1 \text{ km s}^{-1} \lesssim v \lesssim 20 \text{ km s}^{-1}$ .

In addition to mass and speed, the composition of the ions in the plasma cloud can be determined with a time-of-flight mass spectrometer separating the ions according to their mass. The Ulysses dust instrument does not have a time-of-flight mass spectrometer, contrary to the dust instrument on board Cassini (Srama et al. 2004) which is an upgrade of the Ulysses instrument.

## 2.2. Instrument Description

The dust instrument on board Ulysses consists of a cylindrical sensor (with diameter 442 mm and length 301 mm) with channeltron and pre-amplifiers, signal conditioning, and spacecraft interface electronics. The sensor and the charge signals measured upon impact of a dust particle are schematically shown in Figure 2.

The sensor consists of a grid system for the measurement of the particle charge, an electrically grounded hemispherical gold-coated metal target and a negatively biased ion collector grid. A charged dust particle entering the sensor induces a charge in the charge grid which is measured by a charge sensitive amplifier. Once the particle hits the target, it generates electrons and ions which are separated by the electric field of  $-350 \text{ V}$  between the hemisphere and the ion collector. The negative charges (electrons and negative ions,



$Q_E$ ) are collected at the hemisphere and measured by a charge sensitive amplifier. Positive ions ( $Q_I$ ) are collected and measured at the negatively biased ion collector with a charge sensitive amplifier. The ion collector has a transparency of about 40% so that some of the ions can penetrate the ion collector, are further accelerated and detected by an electron multiplier (channeltron). Secondary electrons are produced in the channeltron, amplified, and measured by a charge sensitive amplifier ( $Q_C$ ). Other parameters measured upon impact are the rise times  $t_I$  and  $t_E$  of both the positive and the negative charge pulses  $Q_I$  and  $Q_E$ . The measured time delay  $t_{EI}$  between the electron and ion pulses is used to distinguish true dust impacts from noise events (Baguhl et al. 1993). Dust impacts have time delays of 2 – 44  $\mu\text{s}$ , while mechanical noise has a time delay of milliseconds. The thresholds and dynamic ranges of the various signals measured upon impact are given in Table 1.

A measurement cycle of the instrument can be initiated if one or more of the signals  $Q_E$ ,  $Q_I$  or  $Q_C$  exceeds an adjustable threshold. During normal operation, an event is initiated by the signals  $Q_I$  or  $Q_C$ . Because of high noise rates encountered for the electron channel,  $Q_E$ , this channel was not selected to initiate a measurement cycle.

The parameters of a single recorded event listed in Table 1 are digitised and stored in an Experiment Data Frame. Coincidences between various event signals, event time and sensor pointing direction during the event as well as status information (housekeeping data) are also recorded for each event. These data are transmitted to Earth and, in an initial step, used to determine whether the event was a true dust impact or a noise event. If the measured signals were due to a dust impact, the particle mass  $m$ , and impact speed  $v$  are derived from the instrument calibration. No intrinsic dust charges were derived from the measured  $Q_P$  signals (Section 2.3). More detailed descriptions of the dust instrument, the reduction of the Ulysses dust data and the identification of noise events are given by Grün et al. (1992a,b, 1995b) and Baguhl et al. (1993).

### 2.3. Instrument Calibration

Before an instrument is carried into space, it must be tested on the ground to verify and calibrate its response. The most striking characteristic of dust particles detected in space is their high speed which is typically in the range of 1 – 100  $\text{km s}^{-1}$ . Their sizes are in the range 0.01 – 10  $\mu\text{m}$ . Thus, in order to calibrate a dust instrument to be flown on a space mission, one has to accelerate particles in this size range to comparable speeds.

The only technique with which this speed and mass range is accessible is electrostatic acceleration (Fechtig et al. 1978; Auer 2001). This technique is based on the acquisition

of kinetic energy by a particle of mass  $m$  and positive charge  $q$  falling through a potential difference  $U$ :  $\frac{1}{2}mv^2 = qU$ , where  $v$  is the terminal speed of the particle. Since the acceleration voltage can easily be measured, and  $v$  and  $q$  can be measured with pick-up electrodes, the mass can be calculated for each accelerated particle.

In an electrostatic accelerator only conducting particles can be accelerated. Either the particle material must be a conductor, or the particle must be coated with a conducting material. Materials used for the calibration of the Ulysses detector were iron, carbon and zinc coated silica (Göller and Grün 1989). Calibration experiments for the Cassini dust instrument were also performed with coated latex particles (Stübig et al. 2001; Stübig 2002). Recently, metal and polymer coated particles could also be used for calibration experiments (Hillier et al. 2009, 2014), and first shots with porous particle analogues have been and are currently being attempted (Sterken et al. 2013b, 2015).

The calibration experiments of the Ulysses dust detector were performed at the Heidelberg dust accelerator facility (Göller and Grün 1985, 1989) which is an electrostatic accelerator with a 2 MV van de Graaf high voltage generator. The particles were in the speed range  $1 \text{ km s}^{-1} \leq v \leq 70 \text{ km s}^{-1}$  and in the mass range  $10^{-18} \text{ kg} \leq m \leq 10^{-13} \text{ kg}$ . In addition to three different particle materials, tests with varying impact angles were also performed.

### 2.3.1. *Speed and Mass*

The particle speed can be determined from the rise times  $t_I$  and  $t_E$  of the charge signals measured on the ion collector and on the target. Grün et al. (1995b) measured the rise times of the impact signals as a function of impact speed for three different materials. The signal strength depends moderately on the particle material and also on the impact angle. Neither the particle material nor the impact angle are known for an impinging micrometeoroid. Therefore, averaged calibration curves are used to obtain impact speeds, assuming that the materials used for calibration represent cosmic dust particles of either iron, rock, carbonaceous or CHON composition. Since the two rise times are measured independently, one obtains two (often different) speed values,  $v_{t_I}$  and  $v_{t_E}$ . The impact speed is taken as the geometric mean of both values:  $v = \sqrt{v_{t_I} \cdot v_{t_E}}$ . The typical accuracy of the derived speed  $v$  is a factor of 2.

Once the particle speed has been determined, its charge to mass ratio can be derived from the calibration curves obtained by laboratory impact experiments (Grün et al. 1995b). From these values and the corresponding impact charges  $Q_E$  and  $Q_I$ , two independent estimates of the mass  $m_{Q_E}$  and  $m_{Q_I}$  are derived. The particle mass is usually taken as the geometric

mean  $m = \sqrt{m_{Q_E} \cdot m_{Q_I}}$ . If the speed is well determined, the mass can also be derived with a higher accuracy. The typical uncertainty in the mass  $m$  is a factor of 10. In this paper we derive the grain mass only from the charge  $Q_I$  measured on the ion collector.

The speed dependent measurable mass range of the instrument is shown in Figure 3. During the close Jupiter flyby in 1992 the electronic detection threshold was set to a higher value because an increased noise level was expected (Grün et al. 1995a). In this case the sensitivity was reduced.

Since the charge sensitive amplifiers covered six orders of magnitude in impact charge (and so did the mass range), the upper limit of the calibrated range is also indicated in Figure 3. For larger particles the instrument operated as a threshold detector (saturation range). The calibration covered a speed interval  $2 \text{ km s}^{-1} \lesssim v \lesssim 70 \text{ km s}^{-1}$ . Due to the speed-dependent mass threshold the mass range accessible by the instrument was  $10^{-19} \text{ kg} \lesssim m \lesssim 10^{-9} \text{ kg}$ .

The instrument calibration obtained in the laboratory was confirmed by measurements in the close vicinity of Jupiter’s Galilean moons (Krüger et al. 1999b). The moons are surrounded by clouds of ejecta dust grains kicked-up from their surfaces. The average impact speeds of these, most likely icy, grains were  $6 - 8 \text{ km s}^{-1}$  and were very close to the expected speeds. Particle sizes were  $0.5 - 1.0 \text{ } \mu\text{m}$  (Krüger et al. 2000, 2003), which is within the well calibrated range of the instrument. On the other hand, the jovian dust streams first detected in interplanetary space and later extensively studied in the jovian magnetosphere consist of much smaller and faster particles, far beyond the calibrated range of the instrument (Zook et al. 1996): grain radii were actually about  $10 \text{ nm}$  and their speeds exceeded  $200 \text{ km s}^{-1}$ . These particles strongly interact with the interplanetary and the Jovian magnetic fields (Grün et al. 1998; Flandes et al. 2011), and they originate from Jupiter’s moon Io (Graps et al. 2000). They are not the subject of this paper.

### 2.3.2. Charge

The induced charge signal,  $Q_P$ , is a measure of the intrinsic charge carried by a dust particle entering the dust sensor. For two reasons the induced charge measurement is the most difficult measurement of the dust instrument: 1) Cosmic dust particles are only weakly charged. A surface potential  $U$  results in a dust charge  $q = 4\pi\epsilon_0Us$  for a spherical particle with radius  $s$  ( $\epsilon_0 = 8.854 \times 10^{-12} \text{ A s V}^{-1} \text{ m}^{-1}$ ). For a typical potential of  $U = 5 \text{ V}$ , the smallest particle exceeding the detection threshold has a radius of about  $20 \text{ } \mu\text{m}$ , or, assuming a density of  $3.3 \times 10^3 \text{ kg m}^{-3}$ , a corresponding mass of about  $10^{-10} \text{ kg}$ . The majority of the

particles detected during the Ulysses mission had masses below  $10^{-12}$  kg (Figure 3). 2) The charge grid is the measuring channel most exposed to ambient noise. Thus, analysis of the charge measurements requires careful consideration of the noise. As a consequence, no charges have yet been determined from the Ulysses and Galileo dust data (Svestka et al. 1996).

The Cassini dust instrument is by an order of magnitude more sensitive in  $Q_P$  which led to the detection of the intrinsic charges for several interplanetary particles and for particles in Saturn’s E ring (Kempf et al. 2004, 2006).

#### 2.4. Angular Sensitivity and Sensor Pointing

Ulysses was a spinning spacecraft with a period of five revolutions per minute. The spin axis was the centre line of the craft’s high-gain antenna which normally pointed at Earth, and most of the time the spin axis pointing was within  $1^\circ$  of the nominal Earth direction for data transmission. This small deviation is usually negligible for the analysis of measurements with the dust detector. The Ulysses spacecraft and mission were explained in more detail by Wenzel et al. (1992).

The Ulysses dust sensor had a  $140^\circ$  wide field-of-view with a sensor area of  $1000\text{ cm}^2$  and it was mounted on the spacecraft nearly at right angles ( $85^\circ$ ) to the antenna axis (spacecraft spin axis). Due to this mounting geometry, the sensor was most sensitive to particles approaching from the plane perpendicular to the spacecraft-Earth direction. The detection geometry of the sensor is illustrated in Figure 1. The impact direction of dust particles was measured by the rotation angle,  $\theta$ , which was the sensor viewing direction at the time of a dust impact. During one spin revolution of the spacecraft, the rotation angle scanned through a complete circle of  $360^\circ$ . It was measured in a right-handed system and  $\theta = 0^\circ$  was defined to be the direction closest to ecliptic north. At  $\theta = 90^\circ$  and  $270^\circ$  the sensor axis pointed nearly along the ecliptic plane. When Ulysses was at high ecliptic latitudes, however, the sensor pointing at  $\theta = 0^\circ$  significantly deviated from the actual north direction. During the passages over the Sun’s polar regions, the sensor always scanned through a plane tilted by about  $30^\circ$  from the ecliptic plane and all rotation angles lay close to the ecliptic plane (Figure 1).

The geometric detection probability for dust particles is defined by the sensitivity of the detector for particles impinging from different directions in an isotropic flux of particles. Directions are defined by the impact angle,  $\phi$ , with respect to the sensor axis. The sensitive area as a function of  $\phi$  is basically a cosine function modified by the shielding of the detector

side wall (Grün et al. 1992a). The maximum area of  $0.1 \text{ m}^2$  is found for  $\phi = 0^\circ$ , and the sensor field-of-view is a cone with  $70^\circ$  half angle. The solid angle covered by the detector is  $1.45 \text{ sr}$ . In an isotropic flux, 50% of the particles hit the detector at  $\phi < 32^\circ$ , while the impact direction of a single particle is only known to be somewhere within the  $140^\circ$  wide field-of-view. The average of all the rotation angle arrival directions of dust particles belonging to a stream is known to much higher accuracy than is the impact direction of a single particle.

Because of the mounting of the dust detector almost perpendicular to the spacecraft spin axis, the effective sensor area for dust impacts depends on the angle between the impact direction and the spin axis. The maximum sensitive area of the detector averaged over one spacecraft revolution is  $0.02 \text{ m}^2$  (Grün et al. 1992b).

Laboratory experiments showed that the sensor side wall was as sensitive to dust impacts as the target itself (Willis et al. 2005), and candidates for wall impactors were indeed identified in the Ulysses interstellar dust data (Altobelli et al. 2004). While relaxing directional constraints, the wall impactors are not likely to change our conclusions on grain sizes. The charge  $Q_I$  measured on the ion collector of the dust instrument did not significantly differ between impacts onto the target and the sensor side wall.

## 2.5. Dust Impact Identification

The Ulysses sensor implements a highly reliable coincidence scheme of impact identification. Electrical signals in three independent channels arriving from a single dust impact are measured within less than 1 ms by two different methods (two charge-sensitive amplifiers and one multiplier). The amplitude ratios, the rise times, and the coincidence times are checked with reference to values that were obtained in calibration experiments, and true impacts are separated from noise events, the latter mostly trigger only a single channel.

Each measured signal (noise event or dust impact) was classified according to the strength of its ion charge signal ( $Q_I$ ) into one of six amplitude ranges. Each amplitude range corresponds to roughly one decade in electronic charge  $Q_I$ . In addition, each event was classified into one of four event classes. The event classification scheme, defining the criteria to be satisfied for each class, is given in Baguhl et al. (1993) and Krüger et al. (1999a). This classification scheme was used for a reliable separation of noise events from true dust impacts. Real dust impacts had at least two charge measurements plus additional coincidence criteria that had to be fulfilled (*cf.* Table 1).

Four classes, together with six amplitude ranges, represent 24 separate categories. Each of these categories had its own 8 bit counter. Each signal registered by the dust instrument

(noise event or dust impact) was counted with one of these counters even if the complete data set of the measured impact parameters (charges, rise times, coincidences, impact direction, etc.) was not transmitted to Earth. During periods of very high dust impact rates a small number of data sets was lost due to the limited data transmission rate of Ulysses (see also Section 3). The counter values, however, were always transmitted so that impact rates could be reconstructed.

## 2.6. Dust Instrument Operation

The Ulysses dust detector was operated almost without interruption from launch in 1990 until 2001. Due to decreasing power generation of the radioisotope batteries (RTGs), however, the available electrical power on board the spacecraft became an issue in 2001. Some instruments on board had to be switched off temporarily, and a cycling instrument operation scheme had to be implemented: one or more of the scientific instruments had to be switched off at a time. As a consequence, the dust instrument was switched off repeatedly (Grün et al. 1995a; Krüger et al. 1999a, 2001, 2006a, 2010). After 30 November 2007 the dust instrument remained switched off permanently even though the Ulysses spacecraft operation continued until 30 June 2009.

Degradation of the dust instrument electronics, in particular the channeltron, was continuously monitored during the mission. We observed a channeltron degradation after approximately ten years of operation which was counterbalanced by an increase of the channeltron high voltage. We did not identify any other indications for instrument ageing in the Ulysses dust data. The smooth and rather undegraded behaviour of the Ulysses dust instrument is in contrast to the twin instrument on board Galileo: The electronics of the Galileo instrument suffered severe degradation due to the harsh radiation environment in Jupiter’s magnetosphere (Krüger et al. 2005), nevertheless, the coincidence scheme provided reliable impact identification even then.

## 3. Identification of Interstellar Dust Impactors

During the entire Ulysses mission the full data sets of 6719 dust impacts (containing impact time, impact charges, charge rise times, impact direction etc. for each dust impact, *cf.* Table 1) were successfully transmitted to Earth (Krüger et al. 2010). During most time periods when the dust detector was operated, the impact rates were sufficiently low so that the data sets of all recorded impacts could be transmitted to Earth. Only around

the Jupiter flybys in 1992 and 2004 were very high impact rates recorded so that the data sets of a large fraction of the detected impacts could not be transmitted to Earth during short intervals. All impacts, however, were always counted with the particle counters of the dust instrument (*c.f.*, e.g., Krüger et al. 2006a, for details). During the time intervals of interstellar dust measurements considered in this paper the data sets of all recorded impacts were transmitted.

An analysis of the dynamical properties (flux, impact direction) of the interstellar dust grains detected during the entire Ulysses mission is given by Strub et al. (2015), and theoretical predictions for interstellar dust flux, flow direction and mass distribution for Ulysses are studied by Sterken et al. (2015). In the present work we analyse the mass distribution of the interstellar grains as derived from the entire mission. To this end, we first have to identify the interstellar impactors in the Ulysses data set.

### 3.1. Dust Grain Dynamics

The dynamics of interstellar dust grains in the solar system is dominated by three major forces: solar gravity, solar radiation, and the Lorentz force. Here we briefly discuss the most important aspects for particle motion in the solar system, a more comprehensive discussion is given in the accompanying paper by Sterken et al. (2015).

Micron-sized and sub-micron sized dust particles are susceptible to a pressure exerted by the solar radiation field. Given that the solar radiation expands with the inverse square of the heliocentric distance,  $r$ , the radiation pressure force  $F_{\text{RP}}$  follows the same distance dependence as solar gravity  $F_{\text{grav}}$  (i.e.  $r^{-2}$ ). Hence the ratio  $\beta = F_{\text{RP}}/F_{\text{grav}}$  is constant for a given particle and depends on particle size, optical properties, morphology, etc. The radiation pressure is strongly size-dependent, with a broad maximum for grain sizes approximately comparable to the wavelength of the incident radiation, i.e. for sub-micron grains. For strongly absorbing materials, the  $\beta$  ratio can be larger than one.

Interstellar particles with  $\beta > 1$  are deflected by the solar radiation, leading to an avoidance cone close to the Sun. For  $\beta = 1$  radiation pressure and gravity cancel out and the particles move on straight "undisturbed" trajectories. Particles with  $\beta < 1$  are concentrated downstream from the Sun.

Dust particles in interplanetary space usually carry an electric charge due to photoionization by the solar radiation field, making them susceptible to the Lorentz force exerted by their motion through the interplanetary magnetic field. The field strength, orientation w.r.t. the particle motion and the grains' charge-to-mass ratio,  $Q/m$ , determine the strength of

the Lorentz force. The surface charge of a spherical grain increases linearly with the grain radius,  $a$ , while the mass has an  $a^3$  dependence. Hence, the relative strength of the Lorentz force strongly increases for smaller particles. For a more detailed discussion the reader is referred to Sterken et al. (2015).

For the conditions in interplanetary space the Lorentz force becomes the dominating force for particles smaller than approximately  $a \lesssim 0.1 \mu\text{m}$  (Landgraf 1998, his Fig. 3.5; note that this value strongly depends on heliocentric distance). Particles larger than approximately  $1 \mu\text{m}$  have a low charge-to-mass ratio and low  $\beta$ , and their dynamics is dominated by gravity. In the intermediate size range, radiation pressure makes a significant contribution, and it may even become the dominant force between  $0.1$  and  $0.4 \mu\text{m}$  (Kimura and Mann 1999).

The Lorentz force depends on the 22-year solar (magnetic) cycle, leading to a focussing and defocussing configuration for interstellar dust. Particles with sufficiently high  $Q/m$  are likely not able to penetrate the heliopause (Linde and Gombosi 2000, note that these authors studied only the defocusing phase of the solar cycle).

We ignore the Poynting-Robertson drag force which is due to an aberration effect exerted on dust grains by the solar radiation field. It causes approximately micrometer-sized particles initially orbiting the Sun at 1 AU distance to spiral into the Sun on timescales of  $10^3$  to  $10^4$  years. The interstellar grains traverse the solar system within 20 to 50 years and they spend a much shorter time close to the Sun where the Poynting-Robertson drag is strongest. The resulting grain deflection is very small and thus negligible in our case.

We ignore any rotation of the dust grains that might lead to rotational bursting of the grains. Rotational bursting which might have an affect on the dust mass distribution by creating an excess of small grains, is not expected for interstellar grains in the heliosphere (Misconi 1993; Draine 2011). Similarly, the Yarkovsky effect can be ignored for the interstellar dust grains (Gustafson 1994).

Furthermore, one might expect a contribution from the rotational energy of the grains to the energy released during impact onto the detector target. The rotational energy of micrometer and submicrometer sized grains is 10 to 15 orders of magnitude smaller than the kinetic energy of the grains. Hence, the rotational energy can be completely ignored for the calibration of our impact measurements. We also ignore any other mechanisms of grain destruction (see Frisch et al. 1999, their Sect. 4.4).



### 3.2. Grain selection criteria

The Ulysses dust data contains impacts by interplanetary as well as interstellar grains. Therefore, we have to find selection criteria that allow us to define data sets with a negligible number of impacts from sources other than interstellar. For the identification of the interstellar impactors we have adopted the same selection criteria as Landgraf (1998) and Frisch et al. (1999) and applied them to the entire Ulysses mission. These criteria were based on the following observations that we are reviewing here:

- 1) After its Jupiter flyby in February 1992, Ulysses observed a relatively constant flux of dust particles above and below the ecliptic plane. The approach direction of these grains was opposite to the direction of interplanetary dust during most of the time, except around Ulysses' perihelion. Hence, they appeared to be in retrograde motion about the Sun (Figure 1). If we assume that these grains enter the solar system from close to the upstream direction of the interstellar helium gas as observed by Ulysses, their impact direction is compatible with an origin from outside the solar system.
- 2) Applying the mass and speed calibration of the dust instrument, most particles had impact speeds in excess of the solar system escape speed, also pointing to an origin from outside the solar system.
- 3) The flux of the interstellar particles was independent of ecliptic latitude (Landgraf et al. 2003; Krüger et al. 2007) in contrast to interplanetary dust that is strongly concentrated toward the ecliptic plane and the inner solar system. Dust emanating from the jovian system is concentrated in the vicinity of Jupiter (Grün et al. 1993; Krüger et al. 2006b).

From the above observations we derive the following identification criteria for interstellar grains: From observation #1 we select every impact that was measured when the interstellar helium flow direction was within the  $\pm 70^\circ$  field-of-view of the dust detector. We add for a  $20^\circ$  margin because the sensor side wall turned out to be as sensitive to dust impacts as the target itself (Section 2.4). When Ulysses crossed the ecliptic plane at a heliocentric distance of about 1.3 AU, the impact directions of interstellar and prograde interplanetary grains were not as clearly separated as it was the case during the rest of the Ulysses orbit. We therefore exclude all impacts around perihelion when Ulysses was between  $-60^\circ$  and  $+60^\circ$  ecliptic latitude.

Over the poles of the Sun, Ulysses detected very small particles which were interpreted as fragments of interplanetary grains ejected from the inner solar system by electromagnetic

effects (Hamilton et al. 1996) and solar radiation pressure (Wehry and Mann 1999; Wehry et al. 2004). In order to remove these particles from the data set the measured amplitude of the ion charge signal,  $Q_I$ , had to be more than one order of magnitude above the detection threshold of the dust instrument. Therefore, over the poles of the Sun, at ecliptic latitudes  $|b| \geq 60^\circ$ , we ignore impacts with impact charge amplitudes  $Q_I \leq 10^{-13}$  C.

Around the Jupiter flybys in 1992 and 2004 Ulysses detected collimated streams of dust particles originating from within Jupiter’s magnetosphere (Grün et al. 1993). In order to avoid contamination of the interstellar dust data set, the measurements during the periods of identified jovian dust streams were ignored entirely. The times when the dust streams occurred were given by Baguhl et al. (1993) and Krüger et al. (2006b) and are adopted here.

Finally, a shift in the approach direction of the interstellar grains by about  $40^\circ$  was recognised in 2005 and 2006 (Krüger et al. 2007; Strub et al. 2011, 2015). Therefore in 2005/2006 the nominal band of rotation angles of  $\pm 90^\circ$  within the interstellar helium flow direction was expanded towards larger rotation angles by  $40^\circ$  to take this shift into account (*c.f.* Figure 4).

The selection criteria for the identification of interstellar grains are listed in Table 2. Our criteria are different from those adopted by Strub et al. (2015). Since our aim is to derive the mass distribution of the grains we have to use criteria that do not induce any bias in the mass distribution. Therefore, we did not constrain the measured impact charge,  $Q_I$ , except for short periods over the poles of the Sun (*c.f.* Table 2). We used the observed impact direction of the interstellar grains by constraining the rotation angle. We do not expect to introduce a bias in the mass distribution this way. On the other hand, Strub et al. (2015) analyse the dynamical properties of the grains. For example, to avoid any bias in the measured impact directions these authors did not constrain the rotation angle.

After removing potential impacts by interplanetary particles with the method described above, we identified 987 interstellar grains in the Ulysses data (compared to 526 interstellar grains identified by Strub et al. 2015). The Ulysses interstellar dust data is shown in Figure 4 (subsets of the Ulysses interstellar dust data for different size bins are shown in Figure 8 in the Appendix). This extends the number of detected interstellar grains by more than a factor of three compared to earlier analyses (305 Ulysses impacts between Jupiter flyby in February 1992 and March 1996; Landgraf 1998; Frisch et al. 1999).

The earlier works also considered 309 interstellar dust impacts measured with Galileo. Here we use only the Ulysses data. Inclusion of the Galileo data would extend the entire data set by only approximately 1/3 and, hence, not seriously increase the statistical significance of our results. On the other hand, Landgraf et al. (2000) concluded that the Galileo data set

is likely contaminated with impacts by interplanetary grains. Galileo measured only in the ecliptic plane where a stronger contribution by interplanetary impactors has to be expected, while Ulysses measured out of the ecliptic plane most of the time.

### 3.3. Dust impact speed

The grain impact speed derived from the instrument calibration can be considered as an independent consistency check of our grain selection criteria. Out of the data set of 987 interstellar grains identified by the selection criteria described in Section 3.2 we selected only those grains with a reliable measurement of the charge rise times,  $t_I$  and  $t_E$ , and, hence, a reliable determination of the grain impact speed (i.e. velocity error factor  $VEF < 6$ ; Krüger et al. 2010). This results in a data set of 943 particles. The average impact speed of these grains is  $24 \pm 12 \text{ km s}^{-1}$ , confirming earlier results by Kimura et al. (2003b). Even though this value is very close to the measured speed of the interstellar gas of 23 to  $26 \text{ km s}^{-1}$ , it should not be taken as a discriminator for either of the two values due to the factor or two uncertainty in the measurement of the interstellar dust speed.

From modelling the particle dynamics (e.g. Sterken et al. 2015) the largest grains are expected to have the highest impact speed due to gravitational acceleration, the mid-sized particles with sizes close to the maximum of the  $\beta$  curve have smaller impact speeds, and the smallest particles have variable speeds due to the Lorentz force. The measured average impact speed is in agreement with our hypothesis that the interstellar dust flow is generally coupled with the gas, and that the majority of the grains in our selected data set are indeed of interstellar origin.

### 3.4. Determining the Dust Mass Distribution

The most straightforward determination of the grain mass is based on the laboratory calibration of the dust instrument and relies on the grain impact speed as derived from the measured rise time of the charge signal (*c.f.* Section 2.3). Equation 1 shows that the mass obtained from the impact charge measurement has a strong dependence on the impact speed, with a power law index of approximately 3.5. Given that the speed calibration has a factor of two uncertainty, this yields a factor of ten uncertainty in the derived mass.

A more accurate mass can be derived if the grain impact speed is known by other means. Such a technique was successfully applied earlier to Ulysses interstellar dust measurements by Landgraf et al. (2000) and to Galileo dust measurements of grains ejected from the Galilean

moons (Krüger et al. 2000, 2003). In the present work we apply two similar approaches to determine the impact speed of the interstellar dust grains. Both take into account the change in velocity of an interstellar grain in the heliosphere which can – in principle – easily be determined from the acceleration due to solar gravity and radiation pressure. We neglect the Lorentz force exerted on the grains by interaction with the solar wind magnetic field, which is a good approximation for grains more massive than approximately  $10^{-16}$  kg. The Larmor radii for such particles are on the order of 500 AU in the region traversed by Ulysses, increasing with distance from the Sun (Grün et al. 1994). They are much larger than the length of their interaction with the solar wind.

The relative strength of radiation pressure is expressed as the ratio,  $\beta$ , between the radiation pressure force and the gravitational force (Section 3.1). For sub-micrometer grains radiation pressure can be of the same order ( $\beta \approx 1$ ) or even larger than gravity ( $\beta > 1$ ). We therefore consider two simple cases, following the strategy applied by Landgraf et al. (2000):

- Model 1) The radiation pressure force and gravity acting on a dust grain have exactly the same strength but opposite directions ( $\beta = 1$ , fixed). Therefore, the interstellar grains move through the solar system on straight lines. Their velocity and flow direction remain unchanged. In this case, the impact velocity is given by the difference between the grain velocity at infinity and the spacecraft velocity.
- Model 2) The ratio  $\beta$  depends on the grain size. In this case, the grain velocity is affected by radiation pressure and gravity. We calculate  $\beta$  and the grain velocity for each grain individually. We take  $\beta$  from Kimura and Mann (1999) as a function of grain radius,  $a$ , for compact spherical grains made of astronomical silicates, having a bulk density of  $\rho = 3.3 \times 10^3 \text{ kg m}^{-3}$ . The grain radius, however, is not measured independently by the dust instrument. We therefore have to derive the radius from the grain mass,  $m$ , obtained from the impact charge measurement. The radius of a spherical grain is given by  $a = (3m/(4\pi\rho))^{1/3}$ . Using the grain radius, we can determine the dust velocity in the heliocentric frame and hence the impact velocity onto the sensor target. Then, an improved grain mass can be calculated by inversion of Equation 1. From this mass we determine a new grain radius which gives us a new  $\beta$ , and so forth. This iterative process leads to a value of  $\beta$  in a self-consistent way.

A disadvantage of this second method is its dependence on the detailed properties of the dust grains which are not well known. We therefore apply both models and compare the results. It turned out that  $\beta = 1$  is a good approximation for the majority of the impacts detected with Ulysses and Galileo (Landgraf et al. 2000). For the biggest detected grains and

for the smallest ones, however, this is not a good approximation. Here, the second model is expected to give better results.

For both models we assume an initial velocity of the grains outside the heliosphere of  $23.2 \text{ km s}^{-1}$  (McComas et al. 2012). This value is about 10% smaller than the value of  $26 \text{ km s}^{-1}$  that was earlier adopted by Landgraf et al. (2000). Equation 1 shows that the derived grain masses increase by about 50% due to this reduced impact speed.

We assume an upstream direction of the interstellar dust flow of  $250^\circ$  ecliptic longitude and  $8^\circ$  latitude as was recently derived by Strub et al. (2015). The longitude is somewhat smaller than the value derived by Landgraf (1998,  $259^\circ$ ). Given the large field-of-view of the dust detector, this is well within the measurement uncertainty. For most of the time, except in 2005/06, this initial velocity vector is (1) compatible with the heliocentric speed and the direction of motion of the interstellar grains detected with Ulysses (Grün et al. 1994; Baguhl et al. 1995b), (2) close to the asymptotic velocity vector of the interstellar helium flow detected by Ulysses and IBEX (Witte 2004; McComas et al. 2012, Section 1), and (3) close to the velocity of the Sun with respect to the local interstellar cloud (Lallement and Bertin 1992). In 2005/06 we take a  $40^\circ$  shift in the grain impact direction into account (Strub et al. 2015).

A recent analysis of neutral helium measurements revealed a potential temporal variation of the inflow direction and speed of neutral helium over four decades (Frisch et al. 2013), which was later put into question by Lallement and Bertaux (2014) who found no evidence for such a variation. For the measurement period of the Ulysses interstellar dust measurements this corresponds to a shift of  $2.7^\circ$  over 16 years. Given the large field-of-view of the dust detector (Section 2.4), this value is negligible for our analysis.

## 4. Results

### 4.1. Dust Mass Distribution

The resulting mass distributions for the three cases considered (calibrated impact speed,  $\beta = 1$  (model 1), and  $\beta$  variable self-consistent (model 2)) are shown in Figure 5. They cover a mass range from approximately  $10^{-18} \text{ kg}$  (which is the detection threshold for grains impacting with  $20 \text{ km s}^{-1}$ ) to  $10^{-10} \text{ kg}$  with maxima at about  $10^{-17} \text{ kg}$  to  $10^{-16} \text{ kg}$ . From modelling the extinction of starlight (Mathis et al. 1977; Draine 2009) it is expected that the number of grains per mass interval steeply rises towards smaller grain masses. This is not seen in the in-situ data, instead the mass distribution shows a deficiency of small grains below approximately  $10^{-16} \text{ kg}$  (top panel). This deficiency is most likely due to the interaction of

the grains with the interplanetary magnetic field (Grün et al. 1994). The upper mass limit at approximately  $10^{-11}$  kg is determined by the size of the dust detector: Large grains are much less abundant than small ones so that only very few large grains were detected.

Comparison of the top panel with the two lower panels in Figure 5 shows that the proportion of particles below  $10^{-16}$  kg is increased and the fraction of particles above this limit is reduced when we derive the grain masses from the  $\beta = 1$  model and the self-consistent model for the grain impact speed. A similar result was also found by Landgraf et al. (2000) from the analysis of the Galileo and the smaller Ulysses interstellar dust data sets available at the time. It was explained by being either due to a contamination by interplanetary impactors that might have lower impact speeds than the interstellar grains or by recombination in the impact-generated plasma cloud in the detector.

The mass distributions derived from the two impact speed models ( $\beta = 1$  and the self-consistent model) are very similar, except that the number of grains at the large mass end is even further reduced in the self-consistent model (*c.f.* middle and bottom panels of Figure 5), again confirming earlier results by Landgraf et al. (2000).

We now consider the contributions of grains with different masses to the overall mass density of interstellar dust in the solar system. In Figure 6 we show the mass distribution of interstellar grains as the differential mass density per unit volume (987 particles; see also Frisch et al. 1999). The distribution derived from astronomical observations (Mathis et al. 1977, hereafter MRN) for an interstellar hydrogen density of  $0.22 \text{ cm}^{-3}$  is shown for comparison. Particles with masses below approximately  $10^{-16}$  kg are strongly depleted in the inner heliosphere due to heliospheric filtering, as compared to the interstellar medium. For instance, the density of grains with mass  $10^{-17}$  kg is reduced in the inner heliosphere by about a factor of 90 below the MRN prediction while  $10^{-18}$  kg grains are deficient by three orders of magnitude. At the same time large (approximately  $10^{-14}$  kg) grains are absent in the MRN distribution, but are abundant in the inflowing interstellar dust. It is incompatible with both interstellar elemental abundances and the observed extinction properties of the interstellar dust population (Draine 2009). The Solar System may by chance be located near a concentration of massive grains in the interstellar medium ( $\ll 1$  kpc; Grün and Landgraf 2000).

The existence of interstellar grains larger than approximately  $10^{-16}$  kg as derived from the Ulysses and Galileo data was an important result from the earlier interstellar dust measurements. The largest contribution of the detected grains to the optical cross-section is provided by grains in the range  $10^{-16}$  kg to  $10^{-14}$  kg, while smaller grains below  $10^{-16}$  kg that are believed to dominate the extinction of starlight do not contribute much to the mass density (Landgraf et al. 2000). Such small grains are significantly depleted in the Ulysses

data due to interaction with the interplanetary magnetic field and the heliospheric boundary during certain time intervals (Slavin and Frisch 2008; Slavin et al. 2010). On the other hand, the large grains above  $10^{-16}$  kg provide a significant contribution to the total mass of dust in the interstellar medium, given their large masses and relative abundance.

The total mass density of interstellar grains as derived from the Ulysses in-situ data can be obtained by integrating over the differential distribution shown in Figure 6. This yields a total mass density of  $(2.1 \pm 0.6) \times 10^{-24}$  kg m $^{-3}$  which is a factor of three smaller than the value derived by Landgraf et al. (2000). This value is dominated by the largest particles detected (see Landgraf et al. 2000, their Fig. 7c). The reduced dust density reflects a smaller proportion of the biggest grains detected after 2000, assuming there are no small-scale variations in the dust density in the ambient interstellar medium close to our solar system. Temporal variations in the flux of these large grains are not likely, as they are only marginally affected by the time-variable interplanetary magnetic field. On the other hand, the dust density varies spatially as the large grains are focussed in the downstream direction behind the Sun. When Ulysses moved towards the Sun, a dust density increase by a factor of 1 to 1.5 and a relative increase in interstellar flux by a factor of 2 to 2.5 with respect to the undisturbed incoming density and flux are expected from simulations (Sterken et al. 2015). However, these regions around Ulysses’ perihelion are ignored in the data selection so that this has a minor effect on the derived mass distribution.

#### 4.2. Gas-to-dust mass ratio in the local interstellar cloud

From the total mass density derived from the in-situ measurements we can calculate the gas-to-dust mass ratio in the local interstellar cloud surrounding our solar system. It gives us information about the refractory elements in our local interstellar environment. We adopt a recently determined total hydrogen density of  $n_{\text{H}} = 0.247$  cm $^{-3}$  (i.e. neutral hydrogen density  $n_{\text{HI}} = 0.192$  cm $^{-3}$  and proton density  $n_{\text{p}} = 0.0554$  cm $^{-3}$ ; Slavin and Frisch 2008, their model 26), and a neutral helium density of  $n_{\text{He}} = 0.015$  cm $^{-3}$  (Möbius et al. 2004). Using the total dust mass density derived from the interstellar grains detected with Ulysses (Section 3.4), we find a gas-to-dust mass ratio in the local interstellar cloud of  $R_{g/d} = 193_{-57}^{+85}$ . This value is somewhat higher than the dust density derived from earlier investigations ( $R_{g/d} \sim 94 - 127$ ; Frisch et al. 1999; Landgraf et al. 2000; Kimura et al. 2003b; Altobelli et al. 2004). It should be mentioned that there is some uncertainty in the total hydrogen density. For example, Heerikhuisen and Pogorelov (2011), from heliosphere models, find a somewhat lower value of  $n_{\text{H}} = 0.21 - 0.23$  cm $^{-3}$ . In our analysis, a value of  $n_{\text{H}} = 0.22$  cm $^{-3}$  results in  $R_{g/d} = 172$ .

Gas-to-dust mass ratios calculated from more recent models with improved solar abun-

dances are in the range  $R_{g/d} \sim 149 - 217$  (Slavin and Frisch 2008). Thus, our present analysis is in good agreement with the results obtained from astronomical observations.

### 4.3. Interstellar dust flux

In Figure 7 we show the cumulative mass flux as derived from the Ulysses interstellar dust measurements. Here we show only the self-consistent model for the speed calibration (model 2). For a discussion of the two other alternatives for calibrating the grain masses the reader is referred to Landgraf et al. (2000). The dust flux distribution extends to somewhat larger particles as compared to the earlier analysis by Landgraf et al. (2000) for two reasons: (1) The reduced impact speed in our present analysis leads to larger grain masses, and (2) the dust data set contains about a factor of three more particles so that the dust detector had a higher chance to catch larger particles. The flux of  $10^{-13}$  kg particles is on the order of  $10^{-7} \text{ m}^{-2} \text{ s}^{-1}$ .

## 5. Discussion

The STARDUST mission recently returned samples of contemporary interstellar grains to Earth. Preliminary analysis of a few of these grains extracted from the interstellar collector indicates that their bulk density is rather low (Westphal et al. 2014). Also Sterken et al. (2015) conclude from the simulations in the context of Ulysses observations on low density interstellar dust. The bulk density affects the charge-to-mass ratio for a given size and, hence, the grain interaction with the interplanetary magnetic field.

In our analysis we assumed the grains to be compact, spherical and composed of astronomical silicates with density  $\rho = 3.3 \times 10^3 \text{ kg m}^{-3}$  (Kimura and Mann 1999). We did not consider porous grains for three reasons: (1) the bulk density is not yet well established from the analysis of the STARDUST samples; (2) the laboratory calibration of the Ulysses dust detector was performed solely with compact grains. Only recently are there attempts to calibrate the dust detector with low-density grains with the Heidelberg Dust Accelerator (Sterken et al. 2013b); (3) Finally, the  $\beta$  curves for porous particles are presently under review (Hiroshi Kimura, priv. comm.). Once these prerequisites are fulfilled, it will be possible to do the next major step in deriving a more consistent calibration of the interstellar grain mass distribution, matching also the STARDUST results. We estimate that if the interstellar grains are of low density indeed, their masses would be typically overestimated by one order of magnitude in the Ulysses data (Sterken 2012; Sterken et al. 2015). This would increase



the gas-to-dust ratio calculated in this paper. On the other hand, many big particles, the flux of which peaks around perihelion (Sterken et al. 2015), were left out of the selection (Section 3). This could reduce the gas-to-dust mass ratio. It is not clear at this stage which effect is bigger, and this needs further investigations.

In addition to the well recognized silicate component of interstellar dust, astronomical observations also indicate the existence of carbon grains in interstellar space (Kimura et al. 2003a; Draine 2011). Carbon has a higher albedo (i.e. higher  $\beta$ ) than silicates and is thus more susceptible to radiation pressure. In order to test the influence of a significant carbon component in our Ulysses detections we assumed that all detected grains are composed of carbon, and we used the  $\beta$  curves for compact carbon from Kimura and Mann (1999, their Fig. 1), instead of the silicate data. With this assumption we recalculated the grain masses with our self-consistent model with variable  $\beta$ . This leads to a reduction in the gas-to-dust mass ratio by about 20%. It should be noted, however, that this is a very simple approach which neither takes into account an influence of the grain composition on the calibration of the impact measurements, nor porosity of the grains. Furthermore, we do not know the abundance of carbon grains in the interstellar dust flow yet. The existence of the  $9.7 \mu\text{m}$  and  $18 \mu\text{m}$  infrared features observed in interstellar clouds indicates that silicate grains are abundant in interstellar space which is also consistent with the STARDUST results (Westphal et al. 2014).

Similarly, the entry speed of the interstellar helium into the heliosphere was under debate (Lallement and Bertaux 2014; Wood et al. 2015; McComas et al. 2015). Values of  $23.2 \text{ km s}^{-1}$  and  $26 \text{ km s}^{-1}$ , respectively, were considered. Our model with variable  $\beta$  and an entry speed of the interstellar grains set to this latter value with all parameters unchanged, yields a gas-to-dust mass ratio about 20% higher than derived for the lower entry speed.

Modelling of the interaction of the small interstellar grains with the solar wind magnetic field suggests that the mass distribution changes with time (Landgraf et al. 1999, 2003; Sterken et al. 2013a). Small grains are depleted between mid-1996 and 1999 because of the defocussing configuration of the solar wind magnetic field. The analysis of the Ulysses data suggests such a depletion of the interstellar grains in this time interval. On the other hand, a concentration of big grains is expected in the downstream direction of the interstellar dust flow behind the Sun. Thus, the measured flux of big grains should have increased around Ulysses' perihelion passage when the spacecraft was close to this region. We have ignored this time interval in our analysis because interstellar grains cannot be clearly separated from interplanetary impactors in this period.

We did not consider temporal changes in our analysis of the grain size distribution. Changes in the slope of the mass distribution are discussed in an accompanying paper by

Strub et al. (2015) which revealed temporal and grain-size dependent variations of the measured dust flux and impact direction. Simulations of the dust size and mass distributions for so-called adapted astronomical silicates show some features similar to the observed dust distribution (Sterken et al. 2015).

Dust measurements between 0.3 and 3 AU in the ecliptic plane exist also from Helios, Galileo and Cassini. These data show evidence for distance-dependent alteration of the interstellar dust stream caused by solar radiation pressure, gravitational focussing by the Sun and electromagnetic interaction of the grains with the time-varying interplanetary magnetic field (Altobelli et al. 2003, 2005).

The gas-to-dust mass ratio derived from our analysis is dominated by the largest grains detected. The largest grains, however, are not seriously affected by radiation pressure and electromagnetic forces. The neglect of potentially big interstellar impactors in the inner solar system may lead to an overestimation of the gas-to-dust mass ratio  $R_{g/d}$ . We will address this aspect in detailed simulations of the grain dynamics (Sterken et al. 2015).

## 6. Conclusions

We analysed the mass distribution of interstellar dust grains entering the heliosphere from 16 years of Ulysses in-situ dust measurements obtained between February 1992 and November 2007. Our analysis extends the time period sampling the interstellar dust size distribution in the heliosphere by more than a factor of two compared to previous investigations by Landgraf et al. (2000). A total number of 987 interstellar dust impacts was identified in the Ulysses dust data, thus extending the total interstellar dust data set by a factor of three compared to earlier analyses.

We used a very similar technique as Landgraf et al. (2000), however, with updated properties of the interstellar medium: interstellar dust speed outside the heliosphere of  $23.2 \text{ km s}^{-1}$  (currently under discussion; Lallement and Bertaux 2014), total interstellar hydrogen density of  $0.247 \text{ cm}^{-3}$ , improved ratios of radiation pressure over gravity  $\beta$  for astronomical silicates. We calculated the grain-size dependent variation of the impact speed and impact direction using the dependence of radiation pressure upon particle size from Kimura and Mann (1999), assuming that the grains are composed of astronomical silicates.

Our results confirm the existence of interstellar grains in the heliosphere in the size range from  $0.05 \mu\text{m}$  to above  $1 \mu\text{m}$ . The overall size distribution measured in-situ with Ulysses within 5 AU from the Sun shows a deficiency of small grains below  $0.3 \mu\text{m}$ , compared to astronomically observed interstellar dust in the interstellar medium (Mathis 2000; Draine

2003; Frisch and Slavin 2013). This deficiency can be partially explained by strong heliospheric filtering (Slavin et al. 2012; Sterken et al. 2013a). Up to now, no exact fit between the simulations and the data has proven this, but the general trend can be recognized.

We find a gas-to-dust mass ratio  $R_{g/d} = 193^{+85}_{-57}$ . This value is compatible with gas-to-dust mass ratios derived from observations of sightlines to stars. Our analysis confirms earlier results that ‘big’ (i.e.  $\approx 1 \mu\text{m}$ -sized) interstellar grains exist in the very local interstellar medium which are not easily accessible to astronomical observations (Wang et al. 2014).

We thank the Ulysses project at ESA and NASA/JPL for effective and successful mission operations, and an anonymous referee for improving the presentation of our results. HK is also grateful to Klaus Hornung for valuable discussions during the preparation of this manuscript. This research was supported by the German Bundesministerium für Bildung und Forschung through Deutsches Zentrum für Luft- und Raumfahrt e.V. (DLR, grant 50 QN 9107). HK and PS gratefully acknowledge support by MPI für Sonnensystemforschung. PS acknowledges support by Deutsche Forschungsgemeinschaft (DFG) grant KR 3621/1-1.

*Facilities:* Ulysses.

## A. Appendix

Figure 8 shows the Ulysses interstellar dust data set used in this paper for three different grain size intervals with approximately equal numbers of particles in each figure.

The data shown in Figures 6 and 7 are listed in Tables 3 to 5.

## REFERENCES

- Altobelli, N., Dikarev, V., Kempf, S., Srama, R., Helfert, S., Moragas-Klostermeyer, G., Roy, M., and Grün, E. (2007). Cassini/Cosmic Dust Analyzer in situ dust measurements between Jupiter and Saturn. *Journal of Geophysical Research*, 112:7105.
- Altobelli, N., Grün, E., and Landgraf, M. (2006). A new look into the Helios dust experiment data: presence of interstellar dust inside the Earth’s orbit. *Astronomy and Astrophysics*, 448:243–252.

- Altobelli, N., Kempf, S., Krüger, H., Landgraf, M., Roy, M., and Grün, E. (2005). Interstellar dust flux measurements by the Galileo dust instrument between Venus and Mars orbit. *Journal of Geophysical Research*, 110:7102–7115.
- Altobelli, N., Kempf, S., Landgraf, M., Srama, R., Dikarev, V., Krüger, H., Moragas-Klostermeyer, G., and Grün, E. (2003). Cassini between Venus and Earth: Detection of Interstellar Dust. *Journal of Geophysical Research*, 108:A10, 7–1.
- Altobelli, N., Moissl, R., Krüger, H., Landgraf, M., and Grün, E. (2004). Influence of wall impacts on the Ulysses dust detector in modelling the interstellar dust flux. *Planetary and Space Science*, 52:1287–1295.
- Altobelli, N., Postberg, F., Kimura, H., Tieloff, M., Sterken, V. J., Hsu, S., Hillier, J., Fiege, K., Khawaya, N., Moragas-Kolstermeyer, G., Burton, M., Srama, R., Kempf, S., and Grün, E. (2015). Cassini-CDA Analysis of Interstellar Dust at Saturn. *Science*. submitted.
- Auer, S. (2001). Instrumentation. In Grün, E., Gustafson, B. A. S., Dermott, S. F., and Fechtig, H., editors, *Interplanetary Dust*, pages 385–444. Springer Verlag, Berlin Heidelberg New York.
- Baggaley, W. J., Marsh, S. H., and Close, S. (2007). Interstellar Meteors. In H. Krüger and A. L. Graps, editor, *Dust in planetary systems*, pages 27–32. ESA SP-643.
- Baggaley, W. J. and Neslušan, L. (2002). A model of the heliocentric orbits of a stream of Earth-impacting interstellar meteoroids. *Astronomy and Astrophysics*, 382:1118–1124.
- Baguhl, M., Grün, E., Hamilton, D. P., Linkert, G., Riemann, R., and Staubach, P. (1995a). The flux of interstellar dust observed by Ulysses and Galileo. *Space Science Reviews*, 72:471–476.
- Baguhl, M., Grün, E., and Landgraf, M. (1996). In Situ Measurements of Interstellar Dust with the Ulysses and Galileo Spaceprobes. *Space Science Reviews*, 78:165–172.
- Baguhl, M., Grün, E., Linkert, G., Linkert, D., and Siddique, N. (1993). Identification of ‘small’ dust impacts in the Ulysses dust detector data. *Planetary and Space Science*, 41:1085–1098.
- Baguhl, M., Hamilton, D. P., Grün, E., Dermott, S. F., Fechtig, H., Hanner, M. S., Kissel, J., Lindblad, B. A., Linkert, D., Linkert, G., Mann, I., McDonnell, J. A. M., Morfill, G. E., Polanskey, C., Riemann, R., Schwehm, G. H., Staubach, P., and Zook, H. A. (1995b). Dust measurements at high ecliptic latitudes. *Science*, 268:1016–1020.

- Belheouane, S., Zaslavsky, A., Meyer-Vernet, N., Issautier, K., Mann, I., and Maksimovic, M. (2012). Detection of Interstellar Dust with STEREO/WAVES at 1 AU. *Solar Physics*, 281:501–506.
- Bertaux, J. L. and Blamont, J. F. (1976). Possible evidence for penetration of interstellar dust into the solar system. *Nature*, 262:263–266.
- Czechowski, A. and Mann, I. (2003a). Local interstellar cloud grains outside the heliopause. *Astronomy and Astrophysics*, 410:165–173.
- Czechowski, A. and Mann, I. (2003b). Penetration of Interstellar Grains into the Heliosphere. *Journal of Geophysical Research*, 108:A10, 8038, 10.1029/2003JA009917.
- Dietzel, H., Eichhorn, G., Fechtig, H., Grün, E., Hoffmann, H. J., and Kissel, J. (1973). The HEOS 2 and HELIOS micrometeoroid experiments. *Journal of Physics E Scientific Instruments*, 6:209–217.
- Draine, B. T. (2003). Interstellar Dust Grains. *Annual Review of Astronomy and Astrophysics*, 41:241–289.
- Draine, B. T. (2009). Perspectives on Interstellar Dust Inside and Outside of the Heliosphere. *Space Science Reviews*, 143:333–345.
- Draine, B. T. (2011). *Physics of the Interstellar and Intergalactic Medium*. Princeton University Press.
- Drolshagen, G., Svedhem, H., Grün, E., Grafodatsky, O., and Prokopiev, U. (1999). Microparticles in the geostationary orbit (GORID experiment). *Advances in Space Research*, 23:123–133.
- Fechtig, H., Grün, E., and Kissel, J. (1978). Laboratory Simulation. In McDonnell, J. A. M., editor, *Cosmic Dust*, pages 607–669. Wiley.
- Flandes, A., Krüger, H., Hamilton, D. P., Valdés-Galicia, J. F., Spilker, L., and Caballero, R. (2011). Magnetic field modulated dust streams from Jupiter in interplanetary space. *Planetary and Space Science*. doi:10.1016/j.pss.2011.05.014.
- Friichtenicht, J. F. and Slattery, J. C. (1963). Ionization Associated with Hypervelocity Impact. Technical report, NASA Technical Note D-2091. <http://ntrs.nasa.gov/search.jsp?R=19630005536>.

- Frisch, P. C., Bzowski, M., Livadiotis, G., McComas, D. J., Moebius, E., Mueller, H.-R., Pryor, W. R., Schwadron, N. A., Sokół, J. M., Vallergha, J. V., and Ajello, J. M. (2013). Decades-Long Changes of the Interstellar Wind Through Our Solar System. *Science*, 341:1080–1082.
- Frisch, P. C., Dorschner, J., Geiß, J., Greenberg, J. M., Grün, E., Landgraf, M., Hoppe, P., Jones, A. P., Krätschmer, W., Linde, T. J., Morfill, G. E., Reach, W. T., Slavin, J., Svestka, J., Witt, A., and Zank, G. P. (1999). Dust in the Local Interstellar Wind. *Astrophysical Journal*, 525:492–516.
- Frisch, P. C., Redfield, S., and Slavin, J. D. (2011). The Interstellar Medium Surrounding the Sun. *Annual Review of Astronomy and Astrophysics*, 49:237–279.
- Frisch, P. C. and Slavin, J. D. (2003). The Chemical Composition and Gas-to-Dust Mass Ratio of Nearby Interstellar Matter. *Astrophysical Journal*, 594:844–858.
- Frisch, P. C. and Slavin, J. D. (2013). Interstellar dust close to the Sun. *Earth, Planets, and Space*, 65:175–182.
- Göller, J. R. and Grün, E. (1985). Calibration of the GALILEO/ISPM Dust Detectors with Iron Particles. In Giese, R. H. and Lamy, P., editors, *Properties and Interaction of Interplanetary Dust*, pages 113–115. Reidel, Dordrecht.
- Göller, J. R. and Grün, E. (1989). Calibration of the GALILEO/ULYSSES dust detectors with different projectile materials and at varying impact angles. *Planetary and Space Science*, 37:1197–1206.
- Graps, A. L., Grün, E., Svedhem, H., Krüger, H., Horányi, M., Heck, A., and Lammers, S. (2000). Io as a source of the Jovian dust streams. *Nature*, 405:48–50.
- Grün, E., Baguhl, M., Divine, N., Fechtig, H., Hamilton, D. P., Hanner, M. S., Kissel, J., Lindblad, B. A., Linkert, D., Linkert, G., Mann, I., McDonnell, J. A. M., Morfill, G. E., Polanskey, C., Riemann, R., Schwehm, G. H., Siddique, N., Staubach, P., and Zook, H. A. (1995a). Two years of Ulysses dust data. *Planetary and Space Science*, 43:971–999.
- Grün, E., Baguhl, M., Hamilton, D. P., Kissel, J., Linkert, D., Linkert, G., and Riemann, R. (1995b). Reduction of Galileo and Ulysses dust data. *Planetary and Space Science*, 43:941–951.
- Grün, E., Dikarev, V., Frisch, P. C., Graps, A., Kempf, S., Krüger, H., Landgraf, M., Moragas-Klostermeyer, G., and Srama, R. (2004). Dust in Interplanetary Space and

- in the Local Galactic Environment. In Witt, A. N., Clayton, G. C., and Draine, B. T., editors, *Astrophysics of Dust*, volume 309 of *Astronomical Society of the Pacific Conference Series*, pages 245–263.
- Grün, E., Fechtig, H., Hanner, M. S., Kissel, J., Lindblad, B. A., Linkert, D., Maas, D., Morfill, G. E., and Zook, H. A. (1992a). The Galileo dust detector. *Space Science Reviews*, 60:317–340.
- Grün, E., Fechtig, H., Kissel, J., Linkert, D., Maas, D., McDonnell, J. A. M., Morfill, G. E., Schwehm, G. H., Zook, H. A., and Giese, R. H. (1992b). The Ulysses dust experiment. *Astronomy and Astrophysics, Supplement*, 92:411–423.
- Grün, E., Gustafson, B. E., Mann, I., Baguhl, M., Morfill, G. E., Staubach, P., Taylor, A., and Zook, H. A. (1994). Interstellar dust in the heliosphere. *Astronomy and Astrophysics*, 286:915–924.
- Grün, E., Krüger, H., Graps, A., Hamilton, D. P., Heck, A., Linkert, G., Zook, H., Dermott, S. F., Fechtig, H., Gustafson, B., Hanner, M., Horányi, M., Kissel, J., Lindblad, B., Linkert, G., Mann, I., McDonnell, J. A. M., Morfill, G. E., Polanskey, C., Schwehm, G. H., and Srama, R. (1998). Galileo observes electromagnetically coupled dust in the Jovian magnetosphere. *Journal of Geophysical Research*, 103:20011–20022.
- Grün, E. and Landgraf, M. (2000). Collisional consequences of big interstellar grains. *Journal of Geophysical Research*, 105 no A5:10,291–10,298.
- Grün, E., Staubach, P., Baguhl, M., Hamilton, D. P., Zook, H. A., Dermott, S. F., Gustafson, B. A., Fechtig, H., Kissel, J., Linkert, D., Linkert, G., Srama, R., Hanner, M. S., Polanskey, C., Horányi, M., Lindblad, B. A., Mann, I., McDonnell, J. A. M., Morfill, G. E., and Schwehm, G. H. (1997). South-North and Radial Traverses through the Interplanetary Dust Cloud. *Icarus*, 129:270–288.
- Grün, E., Zook, H. A., Baguhl, M., Balogh, A., Bame, S. J., Fechtig, H., Forsyth, R., Hanner, M. S., Horányi, M., Kissel, J., Lindblad, B. A., Linkert, D., Linkert, G., Mann, I., McDonnell, J. A. M., Morfill, G. E., Phillips, J. L., Polanskey, C., Schwehm, G. H., Siddique, N., Staubach, P., Svestka, J., and Taylor, A. (1993). Discovery of Jovian dust streams and interstellar grains by the Ulysses spacecraft. *Nature*, 362:428–430.
- Gustafson, B. A. S. (1994). Physics of Zodiacal Dust. *Annual Review of Earth and Planetary Sciences*, 22:553–595.
- Hamilton, D. P., Grün, E., and Baguhl, M. (1996). Electromagnetic escape of dust from the solar system. In Gustafson, B. A. S. and Hanner, M. S., editors, *Physics, Chemistry*

- and Dynamics of Interplanetary Dust*, *ASP Conference Series*, volume 104, pages 31–34.
- Heerikhuisen, J. and Pogorelov, N. V. (2011). An Estimate of the Nearby Interstellar Magnetic Field Using Neutral Atoms. *Astrophysical Journal*, 738:29.
- Hillier, J. K., Sestak, S., Green, S. F., Postberg, F., Srama, R., and Trieloff, M. (2009). The production of platinum-coated silicate nanoparticle aggregates for use in hypervelocity impact experiments. *Planetary and Space Science*, 57:2081–2086.
- Hillier, J. K., Sternovsky, Z., Armes, S. P., Fielding, L. A., Postberg, F., Bugiel, S., Drake, K., Srama, R., Kearsley, A. T., and Trieloff, M. (2014). Impact ionisation mass spectrometry of polypyrrole-coated pyrrhotite microparticles. *Planetary and Space Science*, 97:9–22.
- Kempf, S., Beckmann, U., Srama, R., Horanyi, M., Auer, S., and Grün, E. (2006). The electrostatic potential of E ring particles. *Planetary and Space Science*, 54:999–1006.
- Kempf, S., Srama, R., Altobelli, N., Auer, S., Tschernjawski, V., Bradley, J., Burton, M. E., Helfert, S., Johnson, T. V., Krüger, H., Moragas-Klostermeyer, G., and Grün, E. (2004). Cassini between Earth and asteroid belt: first in-situ charge measurements of interplanetary grains. *Icarus*, 171:317–335.
- Kimura, H. and Mann, I. (1999). Radiation pressure on porous micrometeoroids. In Baggaley, W. J. and Porubcan, V., editors, *Meteoroids 1998*, pages 283–286. Astronomical Institute of the Slovak Academy of Sciences.
- Kimura, H., Mann, I., and Jessberger, E. K. (2003a). Composition, Structure, and Size Distribution of Dust in the Local Interstellar Cloud. *Astrophysical Journal*, 583:314–321.
- Kimura, H., Mann, I., and Jessberger, E. K. (2003b). Elemental Abundances and Mass Densities of Dust and Gas in the Local Interstellar Cloud. *Astrophysical Journal*, 582:846–858.
- Krüger, H., Altobelli, N., Anweiler, B., Dermott, S. F., Dikarev, V., Graps, A. L., Grün, E., Gustafson, B. A., Hamilton, D. P., Hanner, M. S., Horányi, M., Kissel, J., Landgraf, M., Lindblad, B., Linkert, D., Linkert, G., Mann, I., McDonnell, J. A. M., Morfill, G. E., Polanskey, C., Schwehm, G. H., Srama, R., and Zook, H. A. (2006a). Five years of Ulysses dust data: 2000 to 2004. *Planetary and Space Science*, 54:932–956.



- Krüger, H., Dikarev, V., Anweiler, B., Dermott, S. F., Graps, A. L., Grün, E., Gustafson, B. A., Hamilton, D. P., Hanner, M. M. S., Horányi, M., Kissel, J., Linkert, D., Linkert, G., Mann, I., McDonnell, J. A. M., Morfill, G. E., Polanskey, C., Schwehm, G. H., and Srama, R. (2010). Three years of Ulysses dust data: 2005 to 2007. *Planetary and Space Science*, 58:951–964.
- Krüger, H., Graps, A. L., Hamilton, D. P., Flandes, A., Forsyth, R. J., Horányi, M., and Grün, E. (2006b). Ulysses jovian latitude scan of high-velocity dust streams originating from the jovian system. *Planetary and Space Science*, 54:919–931.
- Krüger, H. and Grün, E. (2009). Interstellar dust inside and outside the heliosphere. In Linsky, J. and Izmodenov, V. and Möbius, E., editor, *From the outer heliosphere to the local bubble*. Springer Heidelberg.
- Krüger, H., Grün, E., Landgraf, M., Baguhl, M., Dermott, S. F., Fechtig, H., Gustafson, B. A., Hamilton, D. P., Hanner, M. S., Horányi, M., Kissel, J., Lindblad, B., Linkert, D., Linkert, G., Mann, I., McDonnell, J. A. M., Morfill, G. E., Polanskey, C., Schwehm, G. H., Srama, R., and Zook, H. A. (1999a). Three years of Ulysses dust data: 1993 to 1995. *Planetary and Space Science*, 47:363–383.
- Krüger, H., Grün, E., Landgraf, M., Dermott, S. F., Fechtig, H., Gustafson, B. A., Hamilton, D. P., Hanner, M. S., Horányi, M., Kissel, J., Lindblad, B., Linkert, D., Linkert, G., Mann, I., McDonnell, J. A. M., Morfill, G. E., Polanskey, C., Schwehm, G. H., Srama, R., and Zook, H. A. (2001). Four years of Ulysses dust data: 1996 to 1999. *Planetary and Space Science*, 49:1303–1324.
- Krüger, H., Grün, E., Linkert, D., Linkert, G., and Moissl, R. (2005). Galileo long-term dust monitoring in the jovian magnetosphere. *Planetary and Space Science*, 53:1109–1120.
- Krüger, H., Krivov, A. V., and Grün, E. (2000). A dust cloud of Ganymede maintained by hypervelocity impacts of interplanetary micrometeoroids. *Planetary and Space Science*, 48:1457–1471.
- Krüger, H., Krivov, A. V., Hamilton, D. P., and Grün, E. (1999b). Detection of an impact-generated dust cloud around Ganymede. *Nature*, 399:558–560.
- Krüger, H., Krivov, A. V., Sremčević, M., and Grün, E. (2003). Galileo measurements of impact-generated dust clouds surrounding the Galilean satellites. *Icarus*, 164:170–187.
- Krüger, H., Landgraf, M., Altobelli, N., and Grün, E. (2007). Interstellar dust in the solar system. *Space Science Reviews*, 130:401–408.

- Lallement, R. and Bertaux, J. L. (2014). On the decades-long stability of the interstellar wind through the solar system. *Astronomy and Astrophysics*, 565:A41.
- Lallement, R. and Bertin, P. (1992). Northern-hemisphere observations of nearby interstellar gas – possible detection of the local cloud. *Astronomy and Astrophysics*, 266:479–485.
- Landgraf, M. (1998). *Modellierung der Dynamik und Interpretation der In-situ-Messung interstellaren Staubs in der lokalen Umgebung des Sonnensystems*. PhD thesis, Ruprecht-Karls-Universität Heidelberg.
- Landgraf, M. (2000). Modelling the Motion and Distribution of Interstellar Dust inside the Heliosphere. *Journal of Geophysical Research*, 105, no. A5:10,303–10316.
- Landgraf, M., Augustsson, K., Grün, E., and Gustafson, B. A. S. (1999). Deflection of the local interstellar dust flow by solar radiation pressure. *Science*, 286:2,319–2,322.
- Landgraf, M., Baggeley, W. J., Grün, E., Krüger, H., and Linkert, G. (2000). Aspects of the Mass Distribution of Interstellar Dust Grains in the Solar System from in situ Measurements. *Journal of Geophysical Research*, 105, no. A5:10,343–10352.
- Landgraf, M., Krüger, H., Altobelli, N., and Grün, E. (2003). Penetration of the Heliosphere by the interstellar dust stream during solar maximum. *Journal of Geophysical Research*, 108:5–1.
- Linde, T. J. and Gombosi, T. I. (2000). Interstellar dust filtration at the heliospheric interface. *Journal of Geophysical Research*, 105:10411–10418.
- Mann, I. (2010). Interstellar Dust in the Solar System. *Annual Review of Astronomy and Astrophysics*, 48:173–203.
- Mann, I. and Kimura, H. (2000). Interstellar dust properties derived from mass density, mass distribution, and flux rates in the heliosphere. *Journal of Geophysical Research*, 105 No. A5:10,317–10,328.
- Mathis, J. S. (2000). Properties of interstellar dust. *Journal of Geophysical Research*, 105:10269–10278.
- Mathis, J. S., Ruml, W., and Nordsieck, K. H. (1977). The size distribution of interstellar grains. *Astrophysical Journal*, 217:425–433.
- McComas, D. J., Alexashov, D., Bzowski, M., Fahr, H., Heerikhuisen, J., Izmodenov, V., Lee, M. A., Möbius, E., Pogorelov, N., Schwadron, N. A., and Zank, G. P. (2012). The Heliosphere’s Interstellar Interaction: No Bow Shock. *Science*, 336:1291–1295.

- McComas, D. J., Bzowski, M., Frisch, P., Fuselier, S. A., Kubiak, M. A., Kucharek, H., Leonard, T., Möbius, E., Schwadron, N. A., Sokół, J. M., Swaczyna, P., and Witte, M. (2015). Warmer Local Interstellar Medium: A Possible Resolution of the Ulysses-IBEX Enigma. *Astrophysical Journal*, 801:28.
- Misconi, N. Y. (1993). The spin of cosmic dust: Rotational bursting of circumsolar dust in the F corona. *Journal of Geophysical Research*, 98:18951–18961.
- Möbius, E., Bzowski, M., Chalov, S., Fahr, H.-J., Gloeckler, G., Izmodenov, V., Kallenbach, R., Lallement, R., McMullin, D., Noda, H., Oka, M., Pauluhn, A., Raymond, J., Ruciński, D., Skoug, R., Terasawa, T., Thompson, W., Vallergera, J., von Steiger, R., and Witte, M. (2004). Synopsis of the interstellar He parameters from combined neutral gas, pickup ion and UV scattering observations and related consequences. *Astronomy and Astrophysics*, 426:897–907.
- Raizer, Y. P. (1960). Residual ionization of a gas expanding in vacuum. *Sov. Phys. JETP*, 10:411.
- Redfield, S. and Linsky, J. L. (2008). The structure of the Local Interstellar Medium. IV. Dynamics, morphology, physical properties, and implications of cloud-cloud interactions. *Astrophysical Journal*, 673:283–314.
- Slavin, J. D. and Frisch, P. C. (2008). The Boundary Conditions of the Heliosphere: Photoionization Models Constrained by Interstellar and In Situ Data. *Astronomy and Astrophysics*, 491:53–68.
- Slavin, J. D., Frisch, P. C., Heerikhuisen, J., Pogorelov, N. V., Mueller, H.-R., Reach, W. T., Zank, G. P., Dasgupta, B., and Avinash, K. (2010). Exclusion of Tiny Interstellar Dust Grains From the Heliosphere. *Twelfth International Solar Wind Conference*, 1216:497–501.
- Slavin, J. D., Frisch, P. C., Müller, H.-R., Heerikhuisen, J., Pogorelov, N. V., Reach, W. T., and Zank, G. (2012). Trajectories and Distribution of Interstellar Dust Grains in the Heliosphere. *Astrophysical Journal*, 760:46.
- Srama, R., Ahrens, T. J., Altobelli, N., Auer, S., Bradley, J. G., Burton, M., Dikarev, V. V., Economou, T., Fechtig, H., Görlich, M., Grande, M., Graps, A. L., Grün, E., Havnes, O., Helfert, S., Horányi, M., Igenbergs, E., Jeßberger, E. K., Johnson, T. V., Kempf, S., Krivov, A. V., Krüger, H., Moragas-Klostermeyer, G., Lamy, P., Landgraf, M., Linkert, D., Linkert, G., Lura, F., Mocker-Ahltreep, A., McDonnell, J. A. M., Möhlmann, D., Morfill, G. E., Müller, M., Roy, M., Schäfer, G., Schlotzhauer,

- G. H., Schwehm, G. H., Spahn, F., Stübig, M., Svestka, J., Tschernjawski, V., Tuzolino, A. J., Wäsch, R., and Zook, H. A. (2004). The Cassini Cosmic Dust Analyzer. *Space Science Reviews*, 114:465–518.
- Sterken, V. J. (2012). *Filtering of interstellar dust in the heliosphere*. PhD thesis, IGEP, University of Braunschweig, Germany, and MPIK, Heidelberg, Germany, and IRS, University of Stuttgart, Germany.
- Sterken, V. J., Altobelli, N., Kempf, S., Krüger, H., Srama, R., Strub, P., and Grün, E. (2013a). The filtering of interstellar dust in the solar system. *Astronomy and Astrophysics*, 552:A130.
- Sterken, V. J., Altobelli, N., Kempf, S., Schwehm, G., Srama, R., and Grün, E. (2012). The flow of interstellar dust into the solar system. *Astronomy and Astrophysics*, 538:A102.
- Sterken, V. J., Moragas-Klostermeyer, G., Hillier, J. K., Bugiel, S., Srama, R., Armes, S. P., Fielding, L. A., Lovett, J. R., and Grün, E. (2013b). Calibration of impact ionization dust detectors with porous or fluffy dust particles. In *Dusty Visions Workshop, University of Stuttgart, July 17th-19th, 2013*, page 1.
- Sterken, V. J., Strub, P., Krüger, H., von Steiger, R., and Frisch, P. (2015). 16 years of Ulysses Interstellar Dust Measurements in the Solar System: III. Simulations and Data unveil new insights into Local Interstellar Dust. *Astrophysical Journal*, submitted.
- Strub, P., Krüger, H., and Sterken, V. J. (2015). 16 Years of Ulysses Interstellar Dust Measurements in the Solar System: II. Fluctuations in the dust flow from the data. *Astrophysical Journal*. submitted.
- Strub, P., Sterken, V. J., Krüger, H., Grün, E., and Horányi, M. (2011). Interstellar Dust Flow through the Solar System. In Nosenko, V. Y., Shukla, P. K., Thoma, M. H., and Thomas, H. M., editors, *American Institute of Physics Conference Series*, volume 1397 of *American Institute of Physics Conference Series*, pages 385–386.
- Stübig, M. (2002). *New insights in impact ionization and in time-of-flight mass spectroscopy with micrometeoroid detectors by improved impact simulations in the laboratory*. PhD thesis, Ruprecht-Karls-Universität Heidelberg.
- Stübig, M., Schäfer, G., Ho, T.-M., Srama, R., and Grün, E. (2001). Laboratory simulation improvements for hypervelocity micrometeorite impacts with a new dust particle source. *Planetary and Space Science*, 49:853–858.

- Svestka, J., Auer, S., Baguhl, M., and Grün, E. (1996). Measurements of dust electric charges by the Ulysses and Galileo dust detectors. In Gustafson, B. A. and Hanner, M. S., editors, *Physics, Chemistry and Dynamics of Interplanetary Dust, ASP Conference Series*, volume 104, pages 481–484.
- Taylor, A. D., Baggeley, W. J., and Steel, D. I. (1996). Discovery of interstellar dust entering the Earth’s atmosphere. *Nature*, 380:323–325.
- Wang, S., Li, A., and Jiang, B. W. (2014). Modeling the infrared interstellar extinction. *Planetary and Space Science*, 100:32–39.
- Wehry, A., Krüger, H., and Grün, E. (2004). Analysis of Ulysses data: Radiation pressure effects on dust particles. *Astronomy and Astrophysics*, 419:1169–1174.
- Wehry, A. and Mann, I. (1999). Identification of  $\beta$ -meteoroids from measurements of the dust detector onboard the Ulysses spacecraft. *Astronomy and Astrophysics*, 341:296–303.
- Wenzel, K., Marsden, R., Page, D., and Smith, E. (1992). The Ulysses mission. *Astronomy and Astrophysics, Supplement*, 92:207–219.
- Westphal, A. J., Stroud, R. M., Bechtel, H. A., Brenker, F. E., Butterworth, A. L., Flynn, G. J., Frank, D. R., Gainsforth, Z., Hillier, J. K., Postberg, F., Simionovici, A. S., Sterken, V. J., Nittler, L. R., Allen, C., Anderson, D., Ansari, A., Bajt, S., Bastien, R. K., Bassim, N., Bridges, J., Brownlee, D. E., Burchell, M., Burghammer, M., Changela, H., Cloetens, P., Davis, A. M., Doll, R., Floss, C., Grün, E., Heck, P. R., Hoppe, P., Hudson, B., Huth, J., Kearsley, A., King, A. J., Lai, B., Leitner, J., Lemelle, L., Leonard, A., Leroux, H., Lettieri, R., Marchant, W., Oglione, R., Ong, W. J., Price, M. C., Sandford, S. A., Sans Tresseras, J. A., Schmitz, S., Schoonjans, T., Schreiber, K., Silversmit, G., Solé, V. A., Srama, R., Stadermann, F. J., Stephan, T., Stodolna, J., Sutton, S., Trieloff, M., Tsou, P., Tyliczszak, T., Vekemans, B., Vincze, L., Von Korff, J., Wordsworth, N., Zevin, D., Zolensky, M. E., and 30714 Stardust@home dusters (2014). Evidence for interstellar origin of seven dust particles collected by the Stardust spacecraft. *Science*, 345:786–791.
- Willis, M. J., Burchell, M., Ahrens, T. J., Krüger, H., and Grün, E. (2005). Decreased values of cosmic dust number density estimates in the solar system. *Icarus*, 176:440–452.
- Witte, M. (2004). Kinetic parameters of interstellar neutral helium. Review of results obtained during one solar cycle with the Ulysses/GAS-instrument. *Astronomy and Astrophysics*, 426:835–844.

- Witte, M., Banaszekiewicz, H., and Rosenbauer, H. (1996). Recent results on the parameters of interstellar helium from the Ulysses/GAS experiment. *Space Science Reviews*, 78, no. 1/2:289–296.
- Wolf, H., Rhee, J., and Berg, O. E. (1976). Orbital elements of dust particles intercepted by Pioneers 8 and 9. In Elsässer, H. and Fechtig, H., editors, *Interplanetary Dust and Zodiacal Light*, volume 48 of *Lecture Notes in Physics*, Berlin Springer Verlag, pages 165–169.
- Wood, B. E., Müller, H.-R., and Witte, M. (2015). Revisiting Ulysses Observations of Interstellar Helium. *Astrophysical Journal*, 801:62+.
- Zook, H. A., Grün, E., Baguhl, M., Hamilton, D. P., Linkert, G., Linkert, D., Liou, J.-C., Forsyth, R., and Phillips, J. L. (1996). Solar wind magnetic field bending of Jovian dust trajectories. *Science*, 274:1501–1503.

Table 1: Parameters measured by the dust instrument upon impact of a dust particle onto the sensor and related parameters. From Grün et al. (1995b).

Parameter/ digital value	Measured quantity	Range	Accuracy (logarithmic steps)	Related particle parameters
$Q_E/EA$	Negative charge (electrons)	$10^{-14} - 10^{-8} \text{ C}$	48	Mass, speed
$Q_I/IA$	Positive charge (ions)	$10^{-14} - 10^{-8} \text{ C}$	48	Mass, speed
$Q_C/CA$	Positive charge (partially)	$10^{-13} - 10^{-9} \text{ C}$ (channeltron output)	32	Impact identification
$Q_P/PA$	Induced charge positive negative	$10^{-14} - 10^{-12} \text{ C}$ $10^{-14} - 10^{-10} \text{ C}$	16 32	Electric charge
$t_E/ET$	Rise time of negative charge	$10 - 100 \mu\text{s}$	16	Speed
$t_I/IT$	Rise time of positive charge	$10 - 100 \mu\text{s}$	16	Speed
$t_{EI}/EIT$	Time difference negative & positive charge signals	$-5 - 44 \mu\text{s}$	16	Impact identification
$t_{PE}/PET$	Time difference induced & negative charge signals	$1 - 400 \mu\text{s}$	32	Speed

Table 2: Criteria for the identification of interstellar dust grains used in this paper.

Criteria	Time Period/ Spatial Region	Comments
Rotation angle within $\pm 90^\circ$ of interstellar helium flow direction	Entire data set	Sensor target plus side wall
Rotation angle within $\pm 90^\circ$ of interstellar helium flow direction plus $40^\circ$ toward positive rotation angles	2005/2006	Observed shift in rotation angle
$Q_I > 10^{-13}$ C for impacts at ecliptic latitude $ b  \geq 60^\circ$	Sun's polar regions	Removal of electromagnetically accelerated grains
All dust impacts ignored with $ b  < 60^\circ$ around perihelion	Inner solar system	No separation from interplanetary impactors possible
All dust impacts ignored in 39 short time intervals defined by Baguhl et al. (1993) and Krüger et al. (2006b)	1992/1993 and 2002-2005	Jupiter dust streams removal



Table 3: Mass distribution of interstellar grains derived in this paper. The data are shown in Figure 6. Column (1) lists the grain mass, column (2) the mass per logarithmic mass interval and unit volume, columns (3) and (4) give mass interval used for data binning (30 particles per mass bin), and columns (5) and (6) list the  $\sqrt{n}$  error bars.

Mass [kg] (1)	dm/Vdlog(m) [kg m <sup>-3</sup> ] (2)	Err X+ [kg m <sup>-3</sup> ] (3)	Err X- [kg m <sup>-3</sup> ] (4)	Err Y+ [kg m <sup>-3</sup> ] (5)	Err Y- [kg m <sup>-3</sup> ] (6)
1.67E-14	6.62E-25	1.57E-13	1.77E-15	1.10E-24	3.87E-25
1.35E-15	4.50E-25	1.77E-15	1.03E-15	7.44E-25	2.63E-25
8.84E-16	5.04E-25	1.03E-15	7.56E-16	8.34E-25	2.94E-25
6.87E-16	6.45E-25	7.56E-16	6.25E-16	1.07E-24	3.76E-25
5.55E-16	4.16E-25	6.25E-16	4.92E-16	6.88E-25	2.43E-25
4.53E-16	4.91E-25	4.92E-16	4.18E-16	8.13E-25	2.87E-25
3.81E-16	3.66E-25	4.18E-16	3.47E-16	6.07E-25	2.14E-25
3.15E-16	2.93E-25	3.47E-16	2.86E-16	4.85E-25	1.71E-25
2.36E-16	1.08E-25	2.86E-16	1.94E-16	1.80E-25	6.33E-26
1.71E-16	1.17E-25	1.94E-16	1.50E-16	1.94E-25	6.83E-26
1.38E-16	1.57E-25	1.50E-16	1.28E-16	2.61E-25	9.19E-26
1.14E-16	8.94E-26	1.28E-16	1.02E-16	1.48E-25	5.22E-26
9.04E-17	6.71E-26	1.02E-16	8.01E-17	1.11E-25	3.91E-26
7.19E-17	5.94E-26	8.01E-17	6.45E-17	9.83E-26	3.47E-26
5.97E-17	6.78E-26	6.45E-17	5.52E-17	1.12E-25	3.96E-26
4.78E-17	2.97E-26	5.52E-17	4.14E-17	4.92E-26	1.74E-26
3.74E-17	3.29E-26	4.14E-17	3.38E-17	5.44E-26	1.92E-26
3.03E-17	2.50E-26	3.38E-17	2.72E-17	4.14E-26	1.46E-26

Table 4: Table 3 continued.

Mass [kg] (1)	dm/Vdlog(m) [kg m <sup>-3</sup> ] (2)	Err X+ [kg m <sup>-3</sup> ] (3)	Err X- [kg m <sup>-3</sup> ] (4)	Err Y+ [kg m <sup>-3</sup> ] (5)	Err Y- [kg m <sup>-3</sup> ] (6)
2.44E-17	1.96E-26	2.72E-17	2.18E-17	3.24E-26	1.14E-26
1.97E-17	1.70E-26	2.18E-17	1.77E-17	2.82E-26	9.93E-27
1.48E-17	7.24E-27	1.77E-17	1.23E-17	1.20E-26	4.22E-27
1.13E-17	1.20E-26	1.23E-17	1.04E-17	1.99E-26	7.03E-27
9.14E-18	6.22E-27	1.04E-17	8.01E-18	1.03E-26	3.63E-27
7.30E-18	7.01E-27	8.01E-18	6.65E-18	1.16E-26	4.09E-27
6.04E-18	5.55E-27	6.65E-18	5.48E-18	9.19E-27	3.24E-27
5.14E-18	7.11E-27	5.48E-18	4.82E-18	1.18E-26	4.15E-27
4.34E-18	3.68E-27	4.82E-18	3.90E-18	6.10E-27	2.15E-27
3.64E-18	4.58E-27	3.90E-18	3.39E-18	7.58E-27	2.67E-27
3.04E-18	2.49E-27	3.39E-18	2.72E-18	4.12E-27	1.45E-27
2.49E-18	2.46E-27	2.72E-18	2.28E-18	4.08E-27	1.44E-27
1.97E-18	1.23E-27	2.28E-18	1.71E-18	2.04E-27	7.18E-28
1.58E-18	1.77E-27	1.71E-18	1.46E-18	2.94E-27	1.04E-27
9.41E-19	1.95E-28	1.45E-18	6.12E-19	3.23E-28	1.14E-28

Table 5: Cumulated flux distribution of interstellar grains derived in this paper. The data are shown in Figure 7. Column (1) lists the grain mass, column (2) the cumulated flux of grains larger than the given mass, and columns (3) and (4) list the  $\sqrt{n}$  errors.

Mass [kg] (1)	Flux ( $\geq m$ ) [m <sup>-2</sup> s <sup>-1</sup> ] (2)	Err Y+ [m <sup>-2</sup> s <sup>-1</sup> ] (3)	Err Y- [m <sup>-2</sup> s <sup>-1</sup> ] (4)
2.05E-19	7.03E-05	7.26E-05	6.81E-05
6.47E-19	7.03E-05	7.26E-05	6.81E-05
2.05E-18	6.97E-05	7.19E-05	6.75E-05
6.47E-18	6.06E-05	6.27E-05	5.86E-05
2.05E-17	4.75E-05	4.93E-05	4.56E-05
6.47E-17	3.69E-05	3.85E-05	3.53E-05
2.05E-16	2.59E-05	2.73E-05	2.46E-05
6.47E-16	1.63E-05	1.74E-05	1.52E-05
2.05E-15	4.42E-06	4.98E-06	3.86E-06
6.47E-15	1.50E-06	1.82E-06	1.17E-06
2.05E-14	4.99E-07	6.87E-07	3.10E-07
6.47E-14	3.56E-07	5.16E-07	1.97E-07
2.05E-13	7.13E-08	1.43E-07	0.00E+00

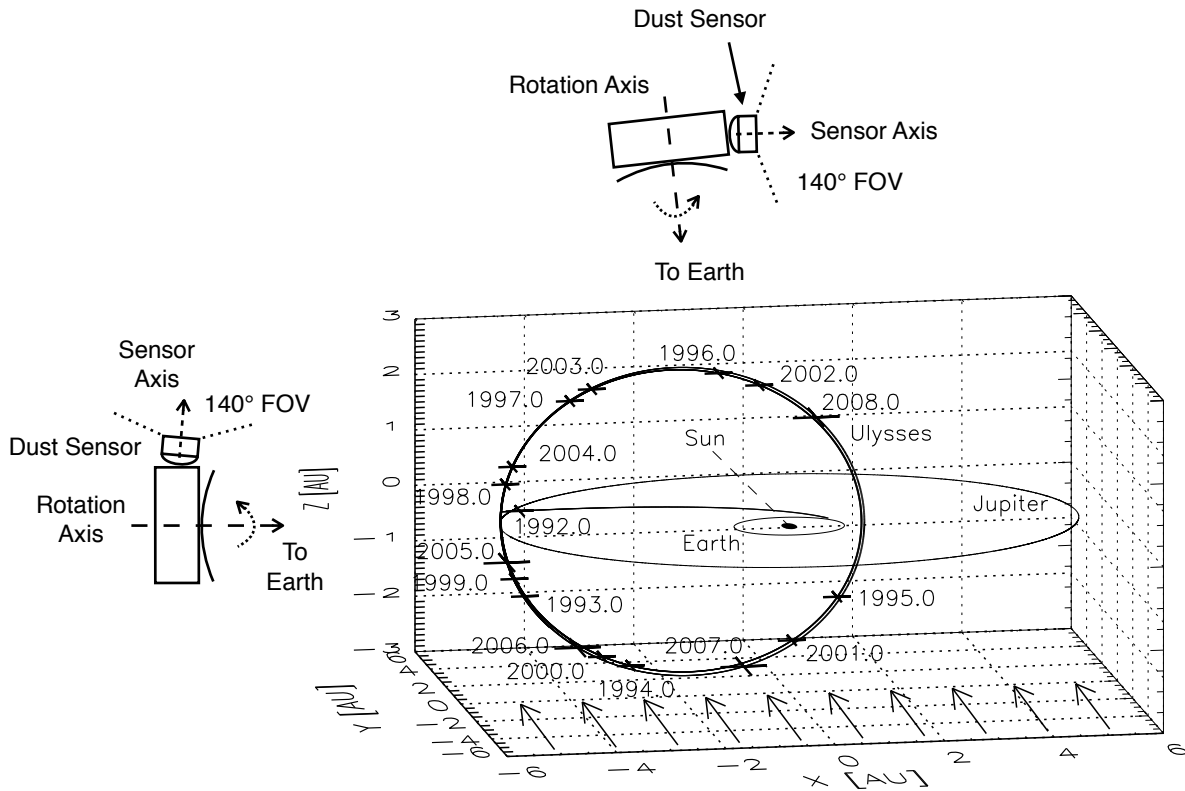


Fig. 1.— The trajectory of Ulysses in ecliptic coordinates with the Sun at the centre. The orbits of Earth and Jupiter indicate the ecliptic plane, and the initial trajectory of Ulysses was in this plane. After Jupiter flyby in early 1992 the orbit was almost perpendicular to the ecliptic plane ( $79^\circ$  inclination). Crosses mark the spacecraft position at the beginning of each year. Vernal equinox is to the right (positive x axis). Arrows indicate the undisturbed interstellar dust flow direction which is within the measurement accuracy co-aligned with the direction of the interstellar helium gas flow. It is almost perpendicular to the orbital plane of Ulysses. The Ulysses spacecraft and the scan orientation of the dust detector are sketched for two positions along the orbit: at aphelion and at the spacecraft's highest ecliptic latitude.

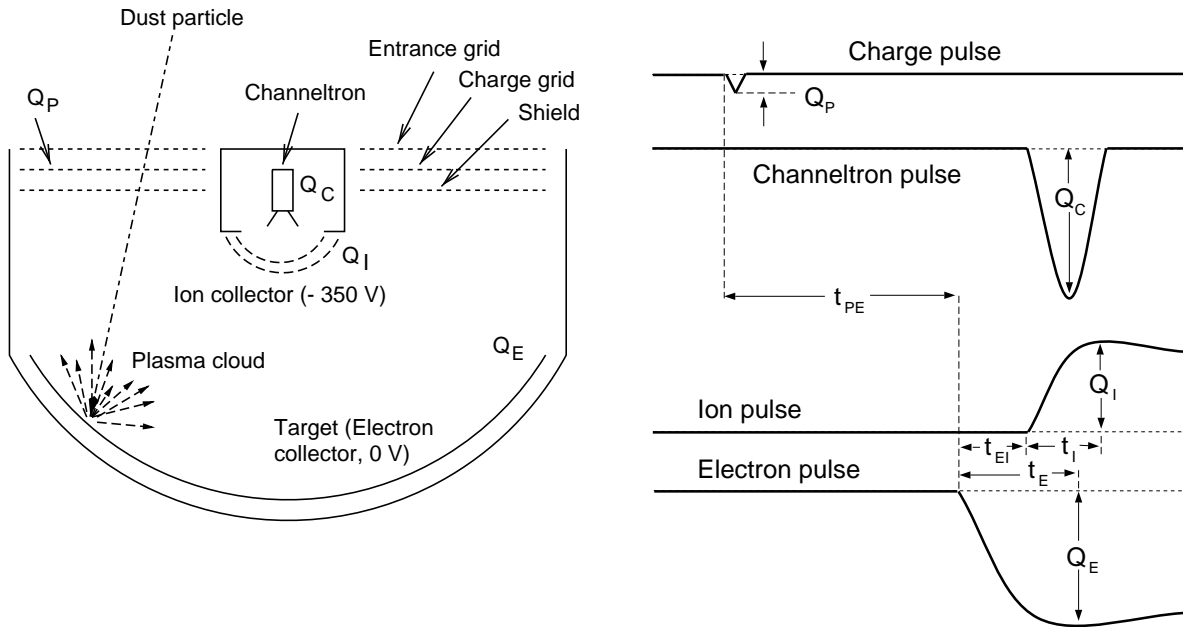


Fig. 2.— Schematic sensor configuration of the Ulysses dust detector (left) and charge signals measured upon impact of a negatively charged dust particle (right). From Grün et al. (1992a).

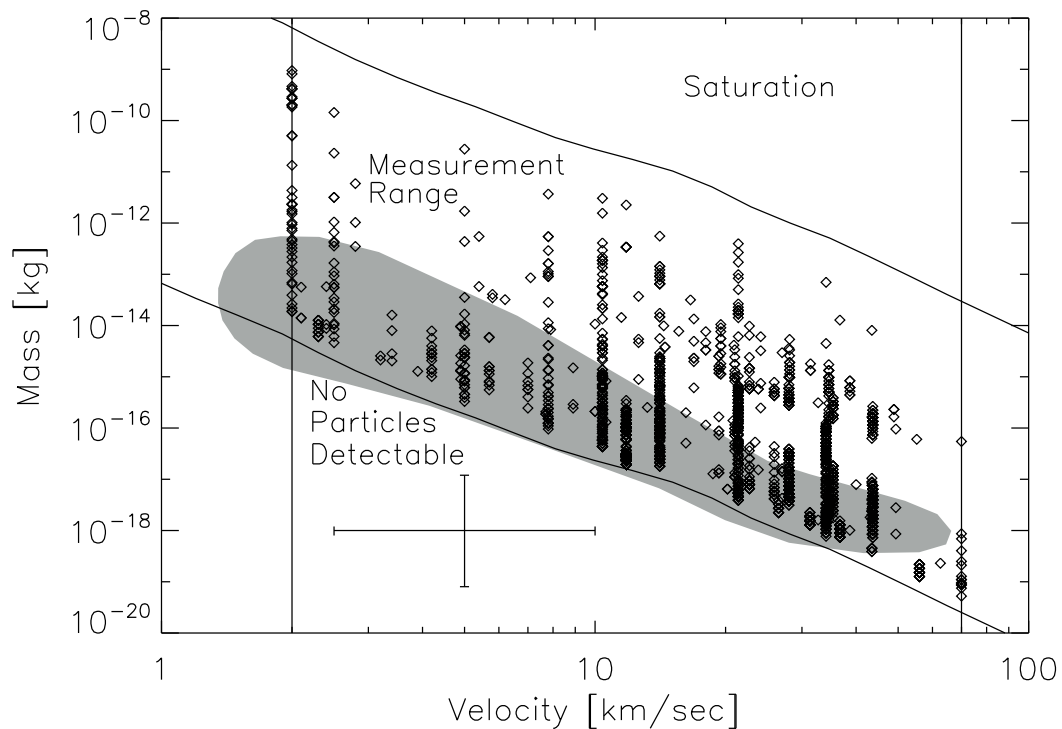


Fig. 3.— Calibrated mass and speed range of the Ulysses dust detector. In the region marked ‘Saturation’ the instrument operates as a threshold detector. The shaded area shows the range where the instrument was calibrated in the laboratory. Below  $2 \text{ km s}^{-1}$  and above  $70 \text{ km s}^{-1}$  speeds and masses cannot be determined. The bottom cross represents typical accuracies of speed and mass values. Plus signs show the calibrated masses and speeds of 2113 particles measured with Ulysses. Jupiter stream particles are not shown as they are actually smaller and faster than the calibrated range of the instrument. Adapted from Grün et al. (1992a).

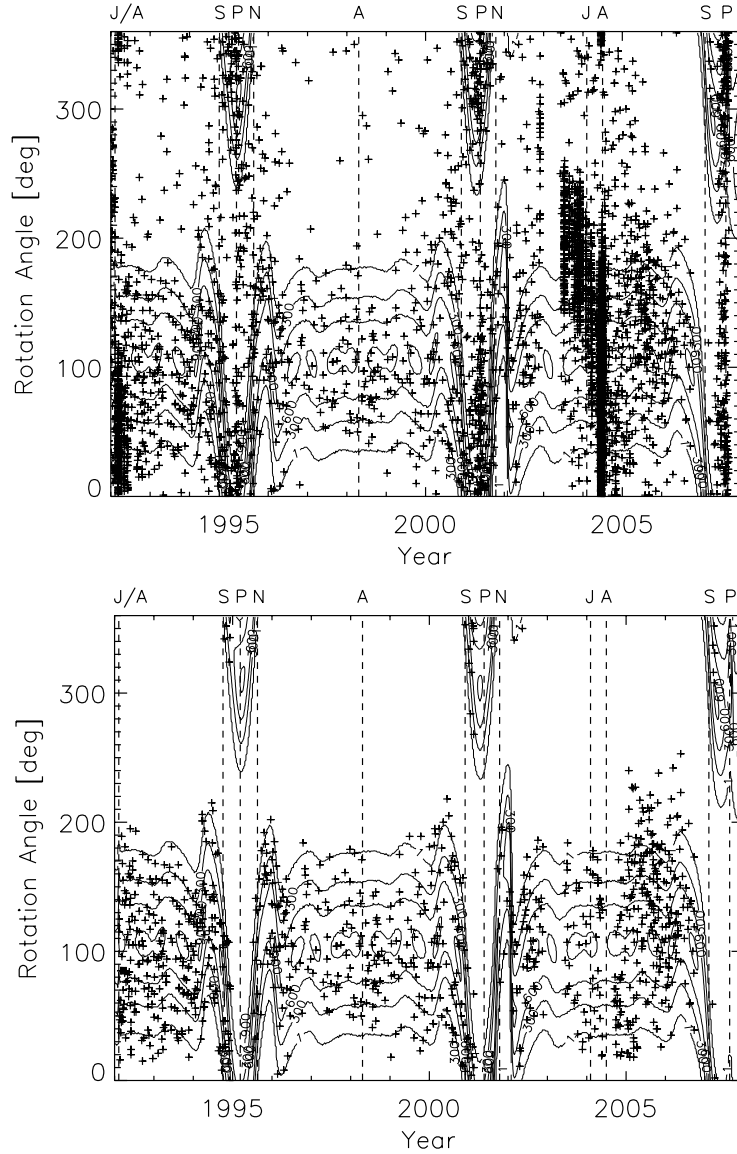


Fig. 4.— Impact direction (rotation angle) vs. time for all dust impacts detected between Jupiter flyby in February 1992 and the end of dust instrument operation in November 2007 (top) and for the identified interstellar dust impactors (bottom). Each cross indicates an individual dust particle impact. Contour lines show the effective sensor area for dust particles approaching from the upstream direction of interstellar helium (McComas et al. 2012). Vertical dashed lines and labels at the top indicate Ulysses’ Jupiter flybys (J), perihelion passages (P), aphelion passages (A), south polar passes (S) and north polar passes of Ulysses (N).

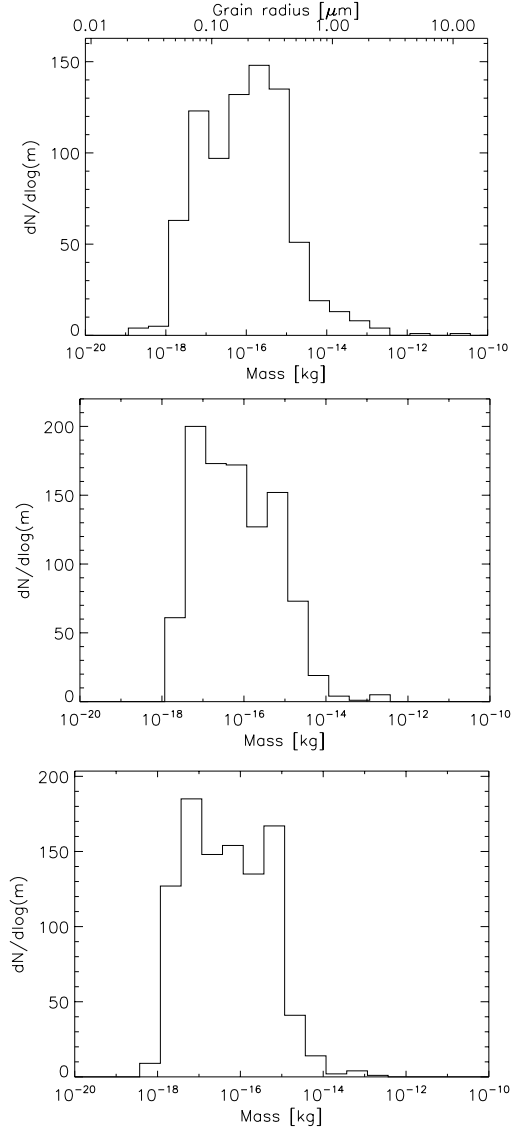


Fig. 5.— Mass distribution of interstellar grains derived from the Ulysses measurements shown as number of particles per logarithmic mass interval for three different cases for the impact speed calculation. *Top panel:* Grain masses derived from the measured impact speeds. Only particles with impact speed  $v > 13 \text{ km s}^{-1}$  were considered (804 particles). *Middle panel:* Masses derived from the  $\beta = 1$  model, taking into account the spacecraft motion (model 1). *Bottom panel:* Masses derived self-consistently (model 2) with accelerated ( $\beta < 1$ ) and decelerated ( $\beta > 1$ ) grains (987 particles for both models). The approximate grain size for spherical particles with density  $\rho = 3.3 \times 10^3 \text{ kg m}^{-3}$  is shown at the top for comparison.



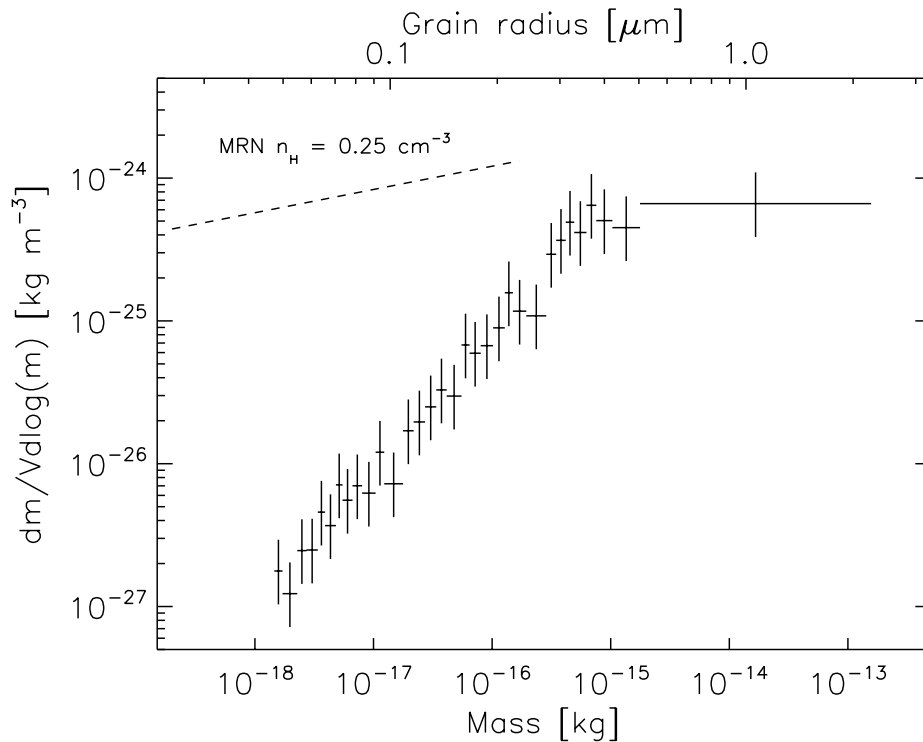


Fig. 6.— Mass distribution of interstellar grains derived from the Ulysses measurements shown as mass per logarithmic mass interval and unit volume (987 particles). The approximate grain size for spherical particles with density  $\rho = 3.3 \times 10^3 \text{ kg m}^{-3}$  is shown at the top for comparison. The dashed line shows the mass distribution derived from astronomical observations (Mathis et al. 1977) for an interstellar hydrogen density of  $0.25 \text{ cm}^{-3}$ . Grain masses were derived from the self-consistent model with accelerated ( $\beta < 1$ ) and decelerated ( $\beta > 1$ ) grains. The data are tabulated in Table 3.

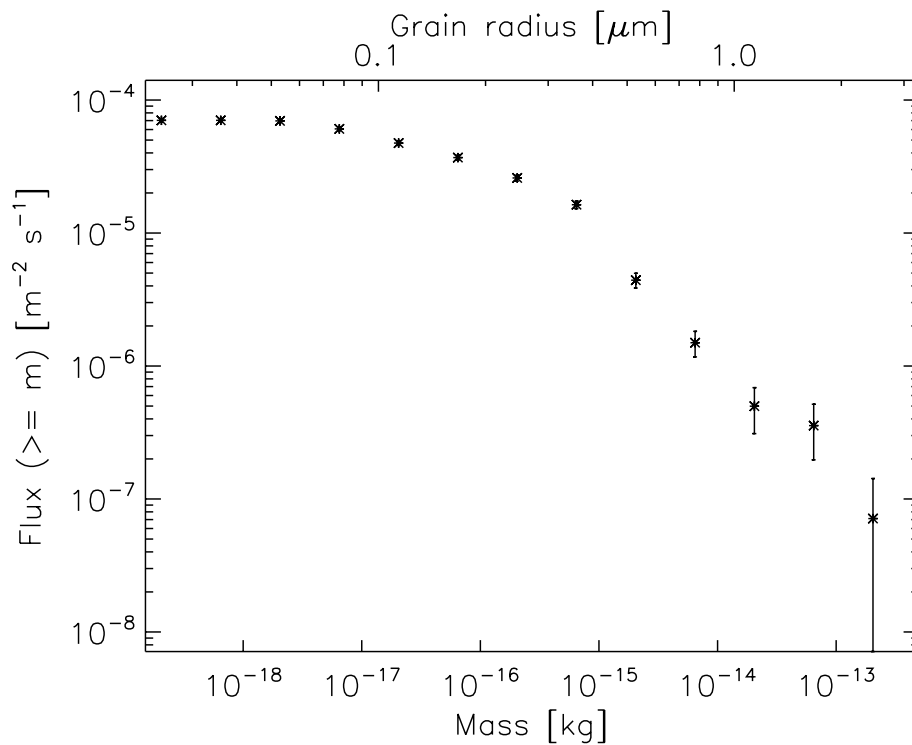


Fig. 7.— Flux of interstellar grains derived from the Ulysses measurements with the self-consistent model with accelerated ( $\beta < 1$ ) and decelerated ( $\beta > 1$ ) grains. The approximate grain size for spherical particles with density  $\rho = 3.3 \times 10^3 \text{ kg m}^{-3}$  is shown at the top for comparison. The data are tabulated in Table 5.

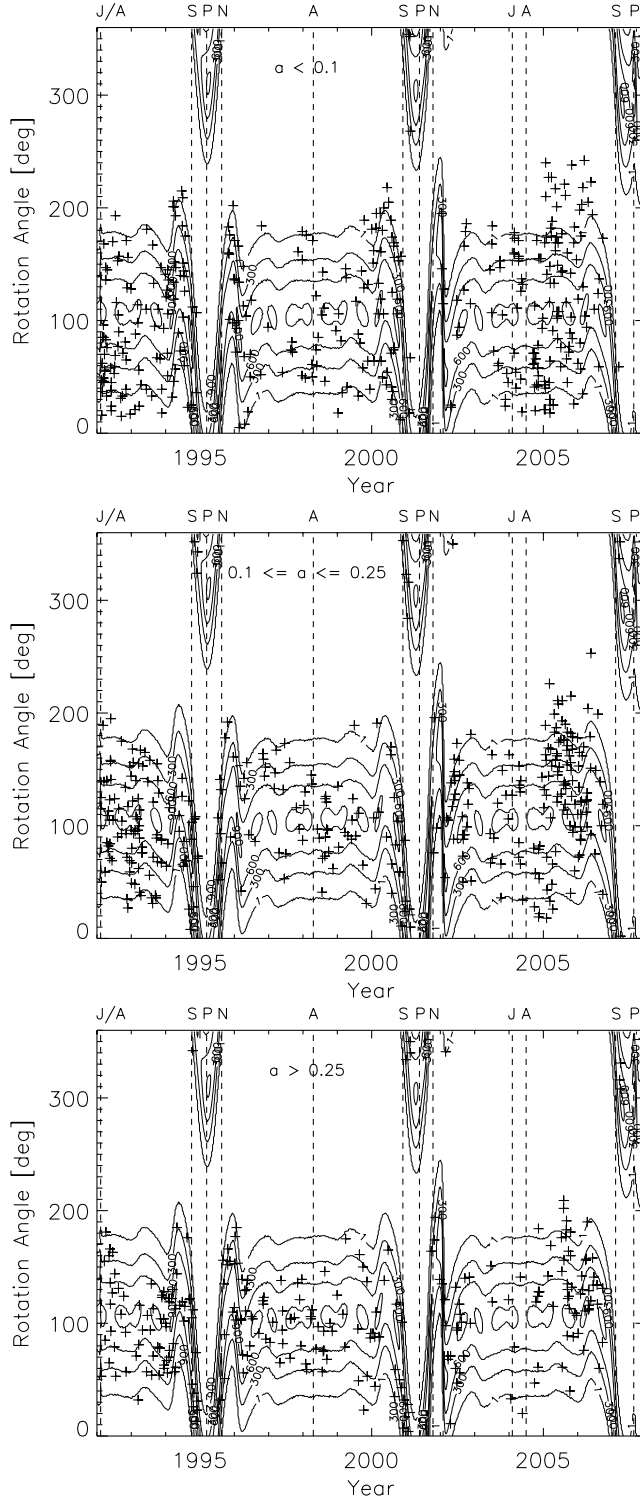


Fig. 8.— Same as Figure 4 but for different subsets of the interstellar dust data (assuming a grain density of  $3.3 \text{ kg m}^{-3}$ ). Top: particles with radius  $a < 0.1 \mu\text{m}$  (363 particles); Middle:  $0.1 \mu\text{m} \leq a \leq 0.25 \mu\text{m}$  (362 particles); Bottom:  $a > 0.25 \mu\text{m}$  (262 particles).